

ARTICLE

Semiclassical transition state theory/master equation kinetics of HO + CO: Performance evaluation

John R. Barker¹  | John F. Stanton²  | Thanh Lam Nguyen² 

¹ Climate and Space Sciences & Engineering, University of Michigan, Ann Arbor, Michigan

² Quantum Theory Project, Department of Chemistry, University of Florida, Gainesville, Florida

Correspondence

John R. Barker, Climate and Space Sciences & Engineering, University of Michigan, Ann Arbor, MI, 48109-2143.

Email: jrbarker@umich.edu

Thanh Lam Nguyen, Quantum Theory Project, Department of Chemistry, University of Florida, Gainesville, FL 32611-7200.

Email: tlam.nguyen@chem.ufl.edu

Dedication: This paper is dedicated to the memory of Joe V. Michael, who steadfastly carried out excellent kinetics experiments throughout his career and always compared the results to existing theories. He was a great example for us all.

Funding information

U.S. Department of Energy, Grant/Award Number: DE-FG02-07ER15884; National Science Foundation, Grant/Award Number: CHE-1748821; U.S. Department of Energy, Grant/Award Number: DE-FG02-07ER15884; National Science Foundation, Grant/Award Number: CHE-1748821

Abstract

Previously, master equation (ME) simulations using semiclassical transition state theory (SCTST) and high-accuracy extrapolated ab initio thermochemistry (HEAT) predicted rate constants in excellent agreement with published experimental data over a wide range of pressure and temperatures ≥ 250 K, but the agreement was not as good at lower temperatures. Possible reasons for this reduced performance are investigated by (a) critically evaluating the published experimental data and by investigating; (b) three distinct ME treatments of angular momentum, including one that is exact at the zero- and infinite-pressure limits; (c) a hindered-rotor model for HOCO that implicitly includes the cis- and trans-conformers; (d) possible empirical adjustments of the thermochemistry; (e) possible empirical adjustments to an imaginary frequency controlling tunneling; (f) including or neglecting the prereaction complex PRC1; and (g) its possible bimolecular reactions. Improvements include better approximations to factors in SCTST and using the Hill and van Vleck treatment of angular momentum coupling. Evaluation of literature data does not reveal any specific shortcomings, but the stated uncertainties may be underestimated. All ME treatments give excellent fits to experimental data at $T \geq 250$ K, but the discrepancy at $T < 250$ K persists. Note that each ME model requires individual empirical energy transfer parameters. Thermochemical adjustments were unable to match the experimental H/D kinetic isotope effects. Adjusting an imaginary frequency can achieve good fits, but the adjustments are unacceptably large. Whether PRC1 and its possible bimolecular reactions are included had little effect. We conclude that none of the adjustments is an improvement over the unadjusted theory. Note that only one set of experimental data exists in the regime of the discrepancy with theory, and data for DO + CO are scanty.

KEYWORDS

CFOUR, chemical activation, data evaluation, energy transfer, high-accuracy extrapolated ab initio thermochemistry (HEAT), HOCO, master equation, MultiWell, OH + CO, semiclassical transition state theory, thermochemistry, transition state theory, tunneling

1 | INTRODUCTION

The title reaction system (Figure 1) is of great importance in at least three different arenas. In the atmosphere, it is the final step in the oxidation of organic compounds. It also helps to regulate the average concentration of OH (hydroxyl) free radicals, which are key chain carriers in atmospheric mechanisms. In combustion, it is the final step in the oxidation of fuels; it is also the principal step that releases chemical energy as heat. In theoretical studies of chemical kinetics and dynamics, the title reaction system is regarded as an important experimental benchmark, because: it is a multiwell reaction system prototype; it consists of a small number of first and second row atoms and is thus amenable to high-level quantum chemistry calculations; and its reactions have been characterized over very wide ranges of both temperature and pressure by many research groups and experimental techniques (see recent critical evaluations Refs. 1–4 of the reaction kinetics data). However, few high-pressure measurements have been reported at temperatures below 200 K and no measurements at all have been reported at temperatures lower than ~ 75 K, although we are aware of experiments using CRESU (a French acronym for Cinétique de Réaction en Ecoulement Supersonique Uniforme, or reaction kinetics in uniform supersonic flow) that are currently underway at extremely low temperatures (Ian Sims, private communication, March 9, 2020).

Theoretical work on this reaction system is so extensive that it cannot be reviewed compactly; instead, to provide access to the literature, we will cite only a few papers. The theoretical work on the HOCO system includes the calculation of optimized stationary points on the potential energy surface (PES) at many levels of theory,^{5–7} full-dimensional PESs constructed using various methods,⁸ classical trajectory calculations,^{9–11} and quantum dynamics calculations.^{12–15} Rate constants, both canonical (ie, thermal) and microcanonical,¹⁶ both with and without quantum tunneling,¹⁷ have been calculated using transition state theory (TST), semiclassical TST (SCTST),^{18,19} and ring polymer molecular dynamics.²⁰ The present paper utilizes SCTST, which was developed by Miller and his colleagues^{21,22} who also showed how its key input parameters can be computed by second-order vibrational perturbation theory and quantum chemistry software. In previous papers,^{23–25} we demonstrated a practical implementation of SCTST and showed that it performs exceptionally well when using input parameters computed using HEAT theory^{26–28} and CFOUR quantum chemistry software.²⁹

To the best of our knowledge, every ab initio study of the title reaction that properly includes pressure effects, including our own,^{18,19} predicts high-pressure limit rate

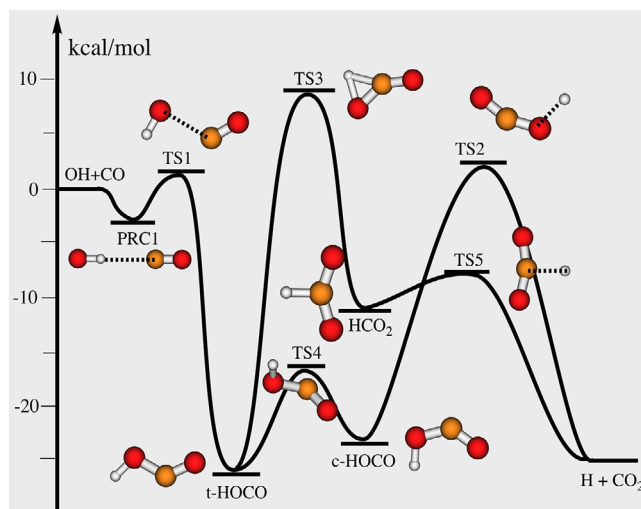


FIGURE 1 PES of the HOCO reaction system¹⁹ [Color figure can be viewed at wileyonlinelibrary.com]

constants, $k_{\infty}(T)$, that are significantly smaller than measured values at $T \lesssim 250$ K. The principal motivation for the present work is to investigate the reasons for this persistent “high-P, low-T” discrepancy.

We begin by critically inspecting the published experimental data. (In future work, we will address the CRESU experiments that are currently underway at very low temperatures.) Evaluation of the published experimental data is followed by investigation of several aspects of the theoretical calculations that might be responsible for the high-P, low-T discrepancy, at least in part. These include three distinct treatments of angular momentum in one-dimensional “1D” master equations, possible errors in the reaction thermochemistry, adjustments to the imaginary frequency, possible bimolecular reactions that might have affected the experimental rate constant measurements, and the influence of the pre-reaction complex that exists in the OH + CO entrance channel (PRC1). The results provide important insights that extend well beyond the present study and have also motivated several improvements in our computer codes, which are used by many researchers.

The present paper is the latest in a series of studies of this reaction system, or its individual components, performed by one or more of the present authors and coworkers.^{18,19,30,31} Paper I¹⁹ reported that a fully ab initio calculation using SCTST, HEAT theory, and rovibrational constants computed using CFOUR produced excellent agreement with experimental rate constants near both the zero and high-pressure limits over the temperature range from ~ 300 to >1000 K.¹⁹ Paper II¹⁸ used results from Paper I to perform master equation calculations over the pressure range between the zero- and high-pressure limits and over the temperature range from 98 to 2000 K. Paper III³⁰ reported both frequency-comb experiments

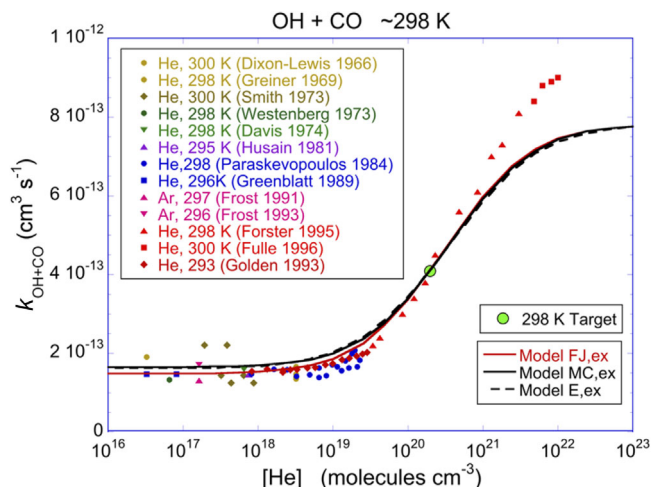


FIGURE 2 Comparison of experiments at ~ 298 K with three explicit models: FJ,ex, MC,ex, and E,ex. All simulations were performed using the “ab initio” HEAT-345Q thermochemistry. (For energy transfer parameters, see Table 2) [Color figure can be viewed at wileyonlinelibrary.com]

and explanatory theory for deuterated OD radicals reacting with CO. Subsequent papers involving one of the present authors were concerned with the spectroscopy of HOCO.³²

The rate constant for this reaction is a function of temperature and $[M]$, the concentration of the bath gas M . At a given temperature, the rate constant is finite at $[M] = 0$ increases with increasing $[M]$ and then approaches a constant value as $[M]$ approaches the high-pressure limit. This behavior is shown in Figure 2, where the experimental data (points) and theoretical models (lines) are discussed in the present work.

Paper II found that master equation calculations performed using the ab initio SCTST microcanonical rate constants (ie, $k(E)$ s) agreed well with experimental pressure-dependent data over a very wide range of pressures and temperatures from ~ 250 to ~ 820 K, based on only a single empirical parameter that describes energy transferred in collisions with the bath gas. However, Paper II noted that while the agreement between theory and experiment near the zero-pressure ($P = 0$) limit is very good to excellent over the entire temperature range, and the agreement near the high-pressure limit is very good at temperatures above ~ 250 K, the theory underpredicts the high-pressure limit at lower temperatures, approaching a factor of $\times 4$ discrepancy between theory and experiment at ~ 100 K. The reason for this discrepancy was not apparent, but several possibilities can be identified and have been investigated in the present work. These include errors in computed thermochemistry, trapping of reactants to form a prereactive complex that then reacts by tunneling to form products,^{33,34} defects in the partition function for OH radical computed at low temperatures,³⁵ possible shortcomings in the mas-

ter equation treatment, and interference by reactions that have not been considered previously.

A second motivation for the present work originated from recent infrared frequency comb experiments on the deuterated isotopologue of the title reaction, OD + CO.^{30,36,37} These are the only experiments in which the reactants, the final products, and the *cis*- and *trans*-DOCO intermediates have all been monitored simultaneously both during and after the reaction. In that work, the experimental equilibrium constant, K_{iso} , for the *cis*-DOCO to *trans*-DOCO isomerization was reported to be $K_{\text{iso}} \approx 5 \pm 2$, while the theoretical prediction from HEAT theory is $K_{\text{iso,th}} \approx 14$.³⁰ The authors suggested that this discrepancy might be due to errors in the infrared absorption coefficients for the two isomers, which were calculated from theory, since they could not be measured. They also suggested that the discrepancy might be due to a ~ 2 kJ mol⁻¹ error in the reaction enthalpy differences. This magnitude of error is surprising, because it is about twice as large as the uncertainty associated with HEAT theory, based on comparisons with Active Thermochemical Tables (ATcT) experimental benchmarks for *trans/cis*-HOCO as well as other small species. HEAT is a high-accuracy composite quantum-chemical method,^{26–28,38} which comprises a number of contributions intended to establish the electronic energy (including nuclear repulsion) of the ground zero-point level of atoms and molecules. These contributions include the Self Consistent Field and CCSD(T) correlation energies, extrapolated to estimate the basis set limit, further corrections for the remaining deficiency of electron correlation treatment at the CCSD(T) level, anharmonic zero-point vibrational corrections estimated with second-order vibrational perturbation theory (VPT2), and further small adjustments for relativistic effects, spin-orbit splitting (relative to the spin-orbit averaged state computed by standard methods), and the adiabatic (diagonal Born-Oppenheimer, or DBOC) correction. For standard molecules comprising the atoms H-Ne, heats of formation inferred from HEAT energies are typically within 1 kJ mol⁻¹ of the exact answer; a roughly similar level of accuracy can be anticipated for transition states without pathological (“multireference”) electronic structure. The latter is upheld for the stationary points (both minima and transition states) involved in the HOCO system; we believe that the relative energies predicted by HEAT for all of these features on the PES are certainly accurate to better than 2 kJ mol⁻¹ (160 cm⁻¹), which represents an uncertainty range that can be regarded as well in excess of 2σ . Some calculations have also used the more recent mHEAT protocol,³⁸ which is both less expensive and less accurate than the more rigorous protocol, with an error range that is approximately doubled.

A fully explicit master equation treatment would require use of a two-dimensional (2D) master equation (ME),

which depends on both total energy and angular momentum (ie, E, J , where J designates both angular momentum and quantum number, depending on context). The 2DME includes a kernel for collisional energy transfer transitions that depends on both variables. Although such treatments were first demonstrated decades ago³⁹⁻⁴³ and exist in improved forms today,³⁹⁻⁴⁶ they require input parameters that involve extensive additional calculations.⁴⁷ Instead of an explicit 2DME, most practical ME calculations utilize various methods for reducing the 2DME to one dimension.^{48,49} We consider three versions of the simpler 1D master equations, which are the most widely used theoretical means for predicting pressure-dependent rate constants. We also present results for a simplified hindered-rotor model that replaces the *cis*-HOCO and *trans*-HOCO intermediates with a single HOCO intermediate containing a 1D hindered internal rotor. Altogether, we compare the results obtained from six different ME treatments.

In the following sections, we first give an overview of how the title reaction proceeds, followed by a description of the quantum chemical and SCTST/1DME calculations, including brief remarks about the six different master equation formulations employed in the present work. These methodology sections are followed by results, discussion, and conclusions.

2 | SURVEY OF PUBLISHED EXPERIMENTAL MEASUREMENTS

Starting with a paper by Ian Smith,⁵⁰ the rate constant for OH + CO has been studied experimentally at many temperatures and pressures of many bath gases by many groups, as reviewed by the NASA³ and IUPAC^{1,51,52} panels. The studies can be conveniently divided into two groups: lower pressures (0-1.5 bar) and higher pressures (1.5 to ~1000 bar). Studies using deuterated hydroxyl radical (OD) and vibrationally excited OH($v=1$) and OD($v=1$) have also been reported, but only at lower pressures. Rate constants at the zero-pressure and infinite-pressure limits ($k_z(T)$ and $k_\infty(T)$, respectively) can only be obtained by extrapolation from rate measurements near the corresponding limits. Studies by many research groups have been performed at relatively low pressures, but only the research group of Jürgen Troe has performed experiments on this reaction at pressures greater than a few bar.^{53,54} By measuring the rate of loss of vibrationally excited reactant (ie, OH($v=1$) and OD($v=1$)), it is also possible to obtain estimates of $k_\infty(T)$,⁵⁵⁻⁵⁸ as described below, but the number of such measurements on the present reaction system is quite limited. Furthermore, this technique is not always free of complications.⁵⁹ Thus $k_z(T)$ is probably better characterized than is $k_\infty(T)$. Brief discussions of experimental data

can be found in reports issued by the NASA and IUPAC data evaluation panels, but the present survey of the data is useful because comparisons with the experimental measurements are of central importance in the present work.

Most of the experiments in the low-pressure regime were performed using flash photolysis or laser flash photolysis in pulse-probe experiments to generate OH (or OD) free radicals from a precursor, and laser induced fluorescence (LIF) from OH (or OD) to monitor the time-dependent concentration of the free radical reactant in the presence of a great excess of CO (ie, under pseudo-first-order conditions), from which rate constants were obtained. Some studies were performed using mass spectrometric detection in fast flow tubes at pressures of a few Torr, but the flash photolysis studies are now regarded as more accurate. Most of the relative uncertainties ($\pm 2\sigma$, or 95% confidence limits) reported for such measurements are of the order of 10% to 20%, but uncertainties as low as $\pm 5\%$ have been reported.

In the lower pressure regime, the recent laser flash photolysis + LIF experiments performed by Liu and Sander⁶⁰ are certainly the most precise ($\pm \sim 5\%$) and possibly the most accurate that have been reported thus far at temperatures from ~220 to 300 K. Although less precise ($\pm \sim 10\%$), results reported by Golden et al⁶¹ and McCabe et al⁶² are also in excellent agreement. These three sets of data are in excellent mutual agreement and can be extrapolated to obtain $k_z(T)$ over the temperature range from ~220 to 300 K with 2σ uncertainties of ~10%. Outside that temperature range, the data from other research groups are less precise and show poorer mutual agreement, but are still very useful.

Liu and Sander⁶⁰ investigated the effect of added traces of O₂ and showed that secondary reactions could regenerate OH radicals and thus produce biexponential decay curves for [OH]. The faster decay component could be identified with the rate constant for OH + CO, and the slower component became apparent only after several half-lives of the first component. None of the other low-pressure studies reported bimolecular decays and the reported rate constants for OH + CO are reasonably consistent with each other, even at temperatures far below 200 K. This suggests that O₂ contamination did not affect the reported rate constants significantly in any of the low-pressure experiments, even at extremely low temperatures.

Direct measurements of OH + CO rate constants in the high-pressure regime have been performed only by Troe, Hippler, and their coworkers.^{53,54} They utilized the saturated LIF technique (SLIF),⁵³ which is based on measuring stimulated emission from OH($v=1$) or OD($v=1$) during the probe pulse of a high-power laser. The SLIF signals are somewhat affected by pressure broadening.⁵³ Forster et al found that when pumping the Q₁(2) line (307.995 nm,

or $32\,468\text{ cm}^{-1}$) of the $\text{OH}(A^2\Sigma, v' = 0) \leftarrow \text{OH}(X^2\Pi, v'' = 0)$ transition in 65 bar of He at 298 K, the pressure-broadened line has a roughly Gaussian shape with full width at half maximum of $\sim 5\text{ cm}^{-1}$. The only chemical species in the OH + CO reaction system that might interfere with the SLIF measurements at this wavelength is the prereactive complex PRC1, but its UV absorption spectrum is shifted higher in energy by about 1000 cm^{-1} ,⁶³ making it unlikely that there is any interference from this source.

Fulle et al⁵⁴ (FHHT) performed high-pressure kinetics measurements from ~ 80 to ~ 820 K. Because of the extreme temperature range, three different sets of photolytic precursors were needed for generating OH and OD radicals, depending on temperature.⁵⁴ Above 250 K, $\text{N}_2\text{O}/\text{H}_2\text{O}/\text{CO}/\text{He}$ mixtures were used. Photolysis of N_2O produced $\text{O}(^1\text{D})$, which reacted with H_2O to produce OH radicals. Near 250 K, the H_2O in the mixture was replaced by H_2 , and at the lowest temperatures (< 250 K), the H_2 was replaced by CH_4 and the N_2O was replaced by O_3 . The OH radical generation in mixtures containing N_2O was relatively “clean,” since the ancillary free radical products (H, or CH_3) did not react rapidly with precursors and interfere with the measurements. However, when O_3 was used, subsequent reaction of the products with O_3 regenerated OH in a free radical chain reaction. FHHT modeled the relevant reactions, however, and showed that the rate constants could be obtained easily by subtracting a background signal caused by OH radical regeneration. The analysis by FHHT also showed that another likely regeneration source of OH is the slow reaction between HOCO and O_3 . This conclusion was confirmed in recent experiments by Bui et al for the deuterated reaction system.³⁰ Despite these complications at temperatures below 250 K, FHHT showed that rate constants could be extracted from the observed LIF decay by simply subtracting a background signal that decays very slowly.

At higher temperatures, when O_3 was not used as a photolytic precursor, the background signal was not present and FHHT obtained total rate constants of the OH (or OD) + CO reaction in three ways. First, the measured pseudo-first-order rate constant in an excess of CO was identified as $k_1(T, \text{He})$. (To simplify notation, “He” denotes “[He]”, the concentration of helium.) Second, high-pressure experiments were performed at temperatures (~ 650 to ~ 820 K) where thermalized HOCO dissociated at a measurable rate, thus producing biexponential decays of the OH concentration, which FHHT analyzed to obtain $k_1(T, \text{He})$ and the equilibrium constant $K_1(T) = k_1(T, \text{He})/k_{-1}(T, \text{He})$. By a theoretical analysis that enabled extrapolation of the measured values of $k_1(T, \text{He})$ to infinite pressure, they obtained values of $k_\infty(T)$. Third, they measured the rate constants for loss of $\text{OH}(v = 1)$ and $\text{OD}(v = 2)$ over the range from 300 to 780 K, obtaining results in excellent agreement with the

previous measurement by Brunning et al⁶⁴ at 298 K. Following the pioneering work of Smith and coworkers,^{56–58} FHHT identified these vibrational deactivation rate constants with $k_\infty(T)$ and found that they are good mutual agreement with the results obtained from extrapolation of the pressure-dependent data. Thus FHHT used two fundamentally different methods for determining $k_\infty(T)$ at temperatures > 250 K, but only one method at lower temperatures. In addition, FHHT developed a semiempirical theoretical model to describe their experiments over the entire ranges of temperature and pressure investigated experimentally. Although their experiments were complicated, FHHT estimated that the results have an accuracy of $\pm 20\%$, which should be regarded as the $\pm 1\sigma$ relative uncertainty (Horst Hippler, private communication, July 3, 2019), independent of temperature and pressure. We are surprised that the uncertainties are not somewhat larger for the extremely high-pressure measurements at extremely low temperatures.

Recently, Bui et al^{30,37} used an infrared frequency comb technique to observe reactants, products, and intermediates in the reaction of OD with CO. The results are qualitatively in accord with current understanding of the reaction system. However, they have deduced a *trans/cis*-DOCO equilibrium ratio that is quantitatively at variance with theoretical calculations.³⁰ Their results for the production rate of *trans*-DOCO are about twice as great as that of *cis*-DOCO.

3 | THEORETICAL METHODS

3.1 | Quantum chemistry

Relative energies of stationary points reported in the previous papers are slightly revised in this work in three aspects: first, DBOCs obtained with the HF method are replaced by those calculated with the CCSD method; second, an old value of 69.5 cm^{-1} for the spin-orbit stabilization of OH (and OD) is replaced by 38.2 cm^{-1} (51.5 cm^{-1} for OD), which is calculated using the Hamiltonian of Hill and Van Vleck⁶⁵ (HVV) for $^2\Pi$ states; third, relativistic corrections to energy are calculated with the both one- and two-electron Darwin method instead of one-electron Darwin method. As seen in Table 1, this revision affects transition states more than minima, but the overall changes are less than $0.22\text{ kcal mol}^{-1}$. As compared to the precise values available from ATcT, the calculated results (which include anharmonic Zero Point Energy corrections) for the reaction enthalpies of *trans*- and *cis*-HOCO agree extremely well, within $0.15\text{ kcal mol}^{-1}$ (see Table 1). This is in fact better from what might (conservatively) be expected from the present calculations, which are unlikely to be in error

TABLE 1 Relative energies (kcal mol⁻¹) of stationary points for the OH + CO reaction system

Species	OH + CO (HEAT-1) ^a	OH + CO (HEAT-3) ^b	OD + CO (HEAT-3) ^b
OH + CO	0.000	0.000	0.000
TS1	0.858	0.775	0.506
TS2	1.950	1.731	2.751
TS3	9.567	9.405	9.966
TS4	-16.640	-16.704	-17.036
t-HOCO	-24.818	-24.883	-25.457
c-HOCO	-23.301	-23.360	-23.830
PRC	-1.389	-1.661	

^a HEAT-1: HEAT-345Q method reported by Tajti et al.²⁶^b HEAT-3: HEAT-345Q reported by Harding et al.²⁸

for systems of this type by more than 0.3 kcal mol⁻¹.²⁶⁻²⁸ Since the reaction barrier heights are not accessible experimentally, a comparison of the barriers is impossible. However, our experience for other similar reactions shows that the barriers calculated with the HEAT method in this work may have an uncertainty similar to that expected for the reaction enthalpies mentioned above. The new relative energies are used in the present work.

The stationary points on the PES (Figure 1) were discussed and compared to the literature in Paper I.¹⁹ One noteworthy point is that lower levels of theory often fail to predict the linear PRCs and transition states found using the high level of theory in the present work. These failures result in erroneously predicting first-order transition states when the high level of theory finds a second-order saddle point, as discussed in Paper I (for a recent example, see Masoumpour and Daryanavard⁶⁶).

3.2 | Chemical kinetics and master equation calculations

The master equation and kinetics calculations were performed using modules in the MultiWell Program Suite.^{67,68} The enthalpies (at 0 K), harmonic frequencies, anharmonicities, and rotational constants that were needed for the calculations were obtained using the CFOUR quantum chemistry code. For most wells (intermediates) and transition states on the PES, densities of states were computed using the MultiWell modules BDENS, or PARADENSUM for fully coupled vibrational models with separable rotations. Densities of states for PRC1, the prereactive complex, were computed using DENSUM, or KTOOLS, based on a separable model for all internal degrees of freedom. Sums of states for fully vibrationally coupled transition states (TSs) that have intrinsic energy barriers were computed using MultiWell modules SCTST, or PARSTST,

which are implementations of SCTST. At each temperature, the location of the “loose” TS for the almost barrierless entrance channel producing PRC1 and the corresponding sum of states were computed using KTOOLS, which is a J-resolved microcanonical implementation of variational transition state theory (VTST). KTOOLS automatically employs Miller’s unified statistical model⁶⁹ when multiple transition states exist along the reaction path. The microcanonical VTST sum of states, which depends on only the total energy E , was obtained by summing the J-resolved sum of states over J. Equilibrium constants and canonical TST rate constants were computed using THERMO, which is a statistical mechanics code for computing thermodynamic quantities. For separable vibrational models, the THERMO calculations were based directly on the molecular constants. For fully coupled vibrational models, THERMO employed partition functions that were precomputed by BDENS, PARADENSUM, SCTST, or PARSTST, which are designed for computing sums and densities of states, rate constants, and partition functions. The method of Hill and Van Vleck⁶⁵ (HVV) for computing energies of spin-orbit states was implemented in THERMO to obtain accurate partition functions for OH(²Π) and other linear species in degenerate electronic states at low temperatures. The implementation in THERMO produces partition functions for OH(²Π) that agree with those from the more elaborate treatment reported by Nguyen et al.³⁵ to within 0.1% from 10 to 1500 K and within 0.6% from 1500 to 2500 K. Complete literature references for all of these modules and the underlying theories are to be found in the *MultiWell User Manual*.⁶⁸

As described elsewhere in detail,^{67,68,70,71} the results of stochastic simulations can be used to obtain rate constants in the following ways. For chemical activation reactions, such as OH + CO ⇌ gHOCO + other products, the essential concept is that when a single OH radical encounters a CO molecule, they enter a well (eg, HOCO) on the PES and at first exist as a nascent transient species, conserving the total energy (and total angular momentum) of the reactant pair, just as in a trajectory calculation. The nascent energy distribution of the transient species is the chemical activation distribution, which can be defined in terms of the reactants, but is more conveniently defined in terms of the reverse reaction and equilibrium constant ($K_{\text{eq}} = k_{\text{forward}}/k_{\text{reverse}}$). The zero of time is set to the assumed instant that the nascent excited HOCO* molecule is first formed. Note that these special simulations for chemical activation reactions do not attempt to replicate experiments in which thermal reactants are depleted by bimolecular reactions. Instead, they simulate the ensemble of initial nascent excited molecules as if all were created simultaneously at $t = 0$. Stochastic trials (10^6 or 10^7 in the present work) are initiated with the HOCO*

initial energy selected by Monte Carlo techniques from the chemical activation energy distribution corresponding to the entrance (capture) channel.

The stochastic simulations are accurate on all timescales, and rate constants can be derived from them when there is a separation of timescales. In chemical activation reactions, the initial energy distribution relaxes very rapidly by collision and reaction during an initial transient period, τ_t , to a new distribution that becomes independent of time; the subsequent reactions have well-defined rate constants. When τ_t is much smaller than the characteristic timescales of the subsequent reactions, processes that occur during τ_t are essentially instantaneous. Based on tests described in Paper II and on further tests in the present work, τ_t in the OH + CO reaction system persists for less than the time needed for 600 collisions to occur, t_{600} . Because τ_t is negligible on the timescale of subsequent reactions, it is convenient to define the bimolecular chemical activation rate constant for forming the i th reaction product as the product $k_{\text{cap}}F_i$, where k_{cap} is the bimolecular rate constant for forming the initial excited transient species and F_i is the probability that, once formed, the transient species will react to produce the i th product during τ_t . Subsequent slower reactions can be described using conventional rate constants (which can also be extracted from the simulations by curve fitting), because the energy distribution has become independent of time.

The rate constants are obtained as follows. At the end of each stochastic trial (ie, at $\tau_t = t_{600}$), the outcome of the trial is recorded. After N_t stochastic trials have been performed, the number, N_i , that terminated in the i th well or product set defines the fraction $F_i = N_i/N_t$, which is used to calculate chemical activation bimolecular rate constants. If the j th product set corresponds to the reactants of the capture reaction (eg, OH + CO), then F_j corresponds to the regenerated reactants. When $i \neq j$, F_i corresponds to the generation of other products, including wells and bimolecular product sets, and the bimolecular chemical activation rate constant for production of the i th product is

$$k_i = k_{\text{cap}} F_i, \quad (1)$$

where k_{cap} is the bimolecular rate constant for capture, which is the high-pressure limit rate constant for the reverse of the reaction that regenerates the reactants: $k_{\text{cap}} = k_{-j,\infty} = k_{j,\infty}/K_j$, where $K_j = k_j/k_{-j}$ at all pressures. For any conditions of pressure and temperature, the rate constants for the bimolecular recombination and its reverse are given by Equations (2a) and (2b), respectively:

$$k_{-j} = k_{\text{cap}} (1 - F_j), \quad (2a)$$

$$k_j = k_{\text{cap}} K_j (1 - F_j) \quad (2b)$$

For unimolecular reactions, the stochastic simulations can replicate laboratory experiments directly. In this case, the simulations are initiated with the energy of the reactant selected from the thermal (canonical) energy distribution and simulations are typically performed for time periods long enough so that some of the reactant has been converted to products at $t > \tau_t$. Following the initial transient period, the time-dependent fraction of initial reactant, $F_j(t)$, and all other $F_i(t)$ can be regarded as proportional to the respective time-dependent concentrations. Rate constants are then obtained by methods familiar from the analysis of experimental data (eg, least squares fitting to an exponential decay over the time for $t > \tau_t$).

The reaction that produces PRC1 is almost barrierless (intrinsic barrier top that is only ~ 0.0218 kcal mol $^{-1}$ above the energy of free OH + CO), thus requiring VTST to locate the position of the TS and compute the rate constant. The variational TS for this entrance channel is designated TSO. The entrance channel was characterized by using a series of constrained geometry optimizations along the reaction path, performed using CCSD(T)/ANO1, which is also used to obtain harmonic frequencies and rotational constants, and single-point calculations for energy using CCSD(T)/ANO2 at the CCSD(T)/ANO1 geometries. PRC1 and all of the structures along the reaction path are linear and in the $^2\Pi$ electronic state. The spin-orbit (SO) constants for PRC1 and at all points along the reaction path were assumed to be the same as that of OH radical, $A_{\text{SO}} = -139.051$ cm $^{-1}$.⁷² This assumption is supported by unpublished calculations (utilizing the spin-orbit CCSD(T) method⁷³) performed by Lan Cheng (private communication, July 3, 2019) and is consistent with the notion that the electronic structure of the OH radical moiety in PRC1 is not affected very much by the CO moiety. The SO enthalpy corrections for OH and PRC1 at their equilibrium geometries were computed using the method of HVV,⁶⁵ resulting in SO corrections of 38.1 and 69.3 cm $^{-1}$, respectively, and a binding energy of $D_0 = 1.661$ kcal mol $^{-1}$ (ie, 581 cm $^{-1}$) for PRC1. This value for D_0 is 171 cm $^{-1}$ higher than the upper limit of $D_0 \leq 410$ cm $^{-1}$ reported by Pond and Lester.⁷⁴ The difference in D_0 energies, which is about twice as large as expected for the HEAT protocol, may be at least partly due to the present simplified treatment of SO coupling in linear PRC1 and linear structures along the reaction path with the HVV method, which neglects the Renner-Teller interactions with the bending modes.⁷⁵ Tests showed that because of its small rotational constant relative to free OH, treating the electronic and rotational degrees of freedom in PRC1 as separable agrees within 0.1% with the HVV treatment from below 20 K to above 2000 K. Because all of the structures along the reaction path have rotational constants even smaller than those of PRC1, the separable approximation was used for all of them.

The rotational constants and harmonic frequencies of the structures along the reaction path forming PRC1 were used as input to KTOOLS to obtain $k(E,J)$ and $G(E,J)$, the microcanonical rate constant and sum of states, respectively, for variational transition state TS0. By summing $G(EJ)$ over quantum number J ,⁷⁶ $G(E)$ was obtained which is compatible with the 1D master equation model that depends only on total energy (the “E” model treatment of angular momentum, described below). The density of states for the PRC1 well was computed by using a separable model consisting of the harmonic frequencies. $G(E)$ for the entrance channel was used by the MULTIWELL master equation code both for generating $k(E)$ s for the entrance channel and for computing the initial chemical activation distribution in the simulations that included PRC1.

For the model that included PRC1, the molecular properties and enthalpies for all species other than PRC1 were assumed to be identical to those used in the models that ignored PRC1. Except for the entrance channel, which was treated using μ VTST, all other microcanonical rate constants were computed using SCTST, as described above. For TS1, the forward barrier height, which is needed for the SCTST calculations, was adjusted to account for the binding energy of PRC1 and to permit quantum tunneling from within the PRC1 well. For this model, the energy grain size was set to 2 cm⁻¹ because of the shallow well depth of PRC1. Stochastic simulations were initiated using the chemical activation energy distribution based on transition state TS0 for the entrance channel. As in Paper II, tests confirmed that the initial transient period never exceeded the time needed for 600 collisions, t_{600} .

Collisional energy transfer in the context of unimolecular reaction systems is a complicated subject, which has been reviewed recently.⁷⁷⁻⁷⁹ For present purposes, we adopt the conventional exponential-down model for the collision step-size distribution:

$$P(U', U) = \exp\left[-\frac{U - U'}{\alpha}\right] \text{ for } U \geq U', \quad (3)$$

where U and U' are the energies prior to, and following a collision, respectively, and parameter α is approximately equal to $\langle \Delta E \rangle_{\text{down}}$, the average energy transferred in deactivation collisions. The probability density for activating collisions is obtained from detailed balance and Equation (3). Although experimental data on large molecule energy transfer show that α is a function of both energy and temperature,⁷⁷ the energy dependence has a negligible effect when the thresholds for competing reactions are close in energy, as in the present reaction system. Because of the differences among the angular momentum treatments, U in Equation (3) is identified with either total energy, E , or active energy, ϵ , as appropriate. As a result,

α then takes on different meanings and has different magnitudes, as discussed below.

3.3 | Master equation models

In all of the present calculations, it is assumed that every nonlinear polyatomic molecule and transition state can be approximately described as a symmetric top that has a 1D rotor (the “K-rotor” with quantum number K) and a 2D rotor (the “J-rotor” with quantum number J).^{80,81} Extensive research supports the conclusion that this approximation is sufficiently accurate for kinetics.^{49,82-84} Because the K quantum number for a symmetric top is not a “good” quantum number, it is also usually assumed that the K -rotor is not adiabatic and the energy of the K -rotor mixes freely with the other active degrees of freedom. Although this is clearly an approximate approach, and the issue remains the subject of active research,⁸⁵⁻⁹² we adopt this assumption in the present work.

For the reasons stated above, the explicit 2DME methods are beyond the scope of the present work and we confine ourselves to three 1DME methods. The 1DME depends equivalently on either total energy E , or active energy ϵ , which is defined as $\epsilon = E - BJ(J+1)$, where B is the rotational constant of the J-rotor. The first two 1DME methods, designated as “E” and “MC,” are based on using either E or ϵ as the independent variable. The third approach, designated as “FJ,” utilizes the simplifying assumption that the distribution over J (for the J-rotor) is “fixed” and does not change with time.⁹³⁻⁹⁵ This “fixed-J” method is exactly equivalent to an explicit 2DME in the absence of collisions (ie, at all times when $P = 0$, or during the brief time interval prior to when a collision changes J). For a given PES, all three methods are, in principle, exact for calculating the rate constants at the high-pressure limit, $k_{\infty}(T)$. The fixed-J method is also exact for calculating the rate constant at the zero-pressure limit, $k_z(T)$, where the two other methods are only approximately correct. All three methods are only approximately correct in the intermediate pressure range, but we show below that all three give accurate descriptions of experimental rate constants when the energy transfer parameters are adjusted empirically.

In the E Model, where total energy E is the independent variable, angular momentum conservation is neglected altogether. Thus, all degrees of freedom, except translation, are assumed to be active. Collisional energy transfer in this formulation refers to transfer of total rovibrational energy, E . In their studies, Miller and coworkers^{76,96} labeled this approach as “E” and we use the same designation.

In the MC model, where ϵ is the independent variable, angular momentum conservation is treated approximately by applying centrifugal corrections to the

microcanonical rate constant, $k(E)$. Marcus⁸⁰ and Waage and Rabinovitch⁸¹ recognized that angular momentum is conserved during the unimolecular reaction of an isolated molecule and assumed that the J-rotor is “adiabatic” while traversing the reaction path,⁴⁹ in contrast to the “active” degrees of freedom, which freely exchange energy among themselves.⁹⁷ However, because the moment of inertia for the J-rotor varies as a function of position along the reaction path while the J quantum number is conserved, the energy associated with the J-rotor varies, making more or less energy available for reaction and thus affecting $k(E)$. To account for the varying rotational constant, Marcus formulated temperature-dependent “centrifugal corrections” to the reaction critical energies. The Marcus centrifugal treatment as implemented by Weston et al¹⁸ is designated “MC” in the present work. The infinite-pressure limit is not affected by the MC treatment and thus remains exact. Collisional energy transfer in this context refers only to the active energy, ϵ , which includes the K-rotor but not the J-rotor.

The FJ model, which was first described by Penner and Forst,^{93,94} has recently been implemented by Nguyen and Stanton.^{68,95} In this approach, it is assumed that J remains fixed at all times, regardless of the occurrence of collisions. This assumption allows one to solve a separate 1DME for every value of J . By averaging over the appropriate initial energy and angular momentum distributions (eg, thermal, chemical activation, etc.) one obtains average rate constants (“expectation values”) from a steady-state treatment, or concentrations as functions of time from a time-dependent master equation approach. Tests show that the time-dependent and steady-state approaches produce identical rate constants. In this “fixed- J ” formulation, the energy transfer parameters refer to the active degrees of freedom, as in the MC Model.

We note that there is another approach, first described by Smith and Gilbert^{48,49} and extended slightly by Miller and coworkers,^{76,96} but not considered in the present work. Their approach is based on the principal assumption that the quantum number J following a collision is completely independent of the initial J' , but trajectory calculations have demonstrated that J and J' are highly correlated,^{44,98} thus invalidating the principal assumption. Furthermore, because this approach is based on corrections to the collisional energy transfer terms of the master equation, it has no utility at the zero-collision limit, which is an important point of reference in the present work.

The HOCO intermediate(s) can be treated explicitly as *cis*-HOCO and *trans*-HOCO (treatment “ex”), or can be treated as a single species that includes a hindered free internal rotation with local energy minima corresponding to the *cis*- and *trans*-geometries (treatment “hr”). The explicit model treats the two isomers as independent

species, which isomerize by tunneling through or passing over the barrier associated with transition state TS4 (Figure 1). All of the vibrations (including the torsion) in each are treated using the usual VPT2 vibrational energy expansion, including all harmonic and X_{ij} anharmonicity terms, the latter of which are quadratic in the $(v + 1/2)$ term expansion.^{23,24} This model has the distinct advantage that *cis*- and *trans*-HOCO can be simulated individually. However, it has the disadvantage that the individual HOCO vibrational densities of states are sparse at low energies, resulting in problems in treating tunneling through a barrier from well to well. This problem arises when population residing in an energy grain in one well tunnels through a barrier to an energy grain in the second well where no energy state resides (an “empty” grain). In our codes, we pragmatically assume that tunneling into an energy grain is forbidden, unless that grain contains at least one ro-vibrational energy state. We think this is reasonable approximation, but it is difficult to test directly, and we considered ways to minimize the occurrence of empty grains.

The number of empty grains can be reduced by increasing the energy grain size, by increasing the density of states, and by using the hindered-rotor (hr) treatment. In the present work, the grain size cannot be increased, because it must be $\leq 5 \text{ cm}^{-1}$ in order to achieve high accuracy at temperatures down to $\sim 100 \text{ K}$. However, the density of states is greatly increased when using the E treatment, since all internal and external rotational states are included. In the HOCO reaction system, this approach eliminates almost all empty grains. The third approach is to use the hr model, which contains only a single well and thus entirely avoids the empty grain issue.

The “hr” model treats HOCO as a single species containing a separable 1D hindered internal rotation with energy levels treated accurately by quantum mechanics, while the remaining vibrational modes are treated using the fully coupled VPT2 expansion and vibrational constants. This model neglects both the anharmonic coupling between the internal rotation and the other vibrations and the coupling between the internal and external rotations. Tests comparing a fully coupled vibrational model to the “hr” model indicate that anharmonic intermode coupling affects the computed rate constant by $\sim 10\%$ at 100 K . The effects of coupling between the hindered internal rotation and the external rotations are neglected for these kinetics calculations. A limitation of this model is that it cannot treat *cis*- and *trans*-HOCO individually; only the sum of the two can be simulated. Effectively, it is assumed that the microcanonical *cis*-*trans* equilibrium is established more rapidly than any other process. Inspection of Figure 3 and other similar tests shows that this assumption is quite accurate for the OH + CO reaction system, because of the extremely

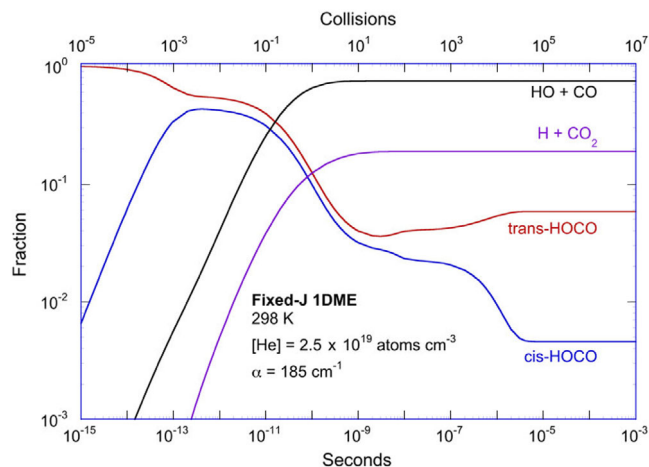


FIGURE 3 Relative concentrations versus time for the HO + CO chemical activation reaction [Color figure can be viewed at wileyonlinelibrary.com]

large $k(E)$ s at energies near and above the isomerization barrier.

By combining the three treatments of angular momentum with the explicit (“ex”) and hindered rotor (“hr”) treatments, we consider six ME models, designated MC,ex, MC,hr; E,ex, E,hr; and FJ,ex, FJ,hr (Figure 4). All three angular momentum treatments are exactly correct at the infinite-pressure limit, and the FJ treatment is also exactly correct at the zero-pressure limit; all three are only approximately correct in the pressure falloff regime and require empirical energy transfer parameters.

As shown in Figure 4, Model MC,ex is the most similar to the model used in our previous work.¹⁸ In our previous work tunneling to empty energy grains was allowed, and we subsequently discovered that the computer code did not always conserve probability exactly when simulating collisional thermalization of the excited HOCO at ener-

gies below the energy of TS4, the isomerization transition state. This problem did not appear to affect the chemical activation simulations, however, which mostly were confined to energies above TS4, where empty grains are rare. An important motivation for the present work is to determine whether the empty grain issue has a perceptible effect on the results.

4 | RESULTS AND DISCUSSION

The PES stationary points and connectivity are shown in Figure 1. First, we consider a model that ignores the existence of the weakly bound prereactive complex PRC1, as was done in Papers I and II. To guide the discussion, we consider simplified thermal reaction mechanisms, as follows, but accurate models will require microcanonical rate constants and appropriate averaging.



where the asterisk denotes ro-vibrational excitation. Reaction (–c) is neglected because it is much slower than the other reactions controlling $[\text{HOCO}^*]$ at low temperature.

By using the pseudo-steady-state approximation for the concentration of HOCO^* , the general rate constant for loss of OH and CO is obtained:

$$k = \frac{k_a(k_b + k_c[\text{M}])}{k_{-a} + k_b + k_c[\text{M}]}, \quad (4)$$

where $[\text{M}]$ is the concentration of the bath gas, M. At zero pressure, when $[\text{M}] = 0$, the rate constant for loss of OH

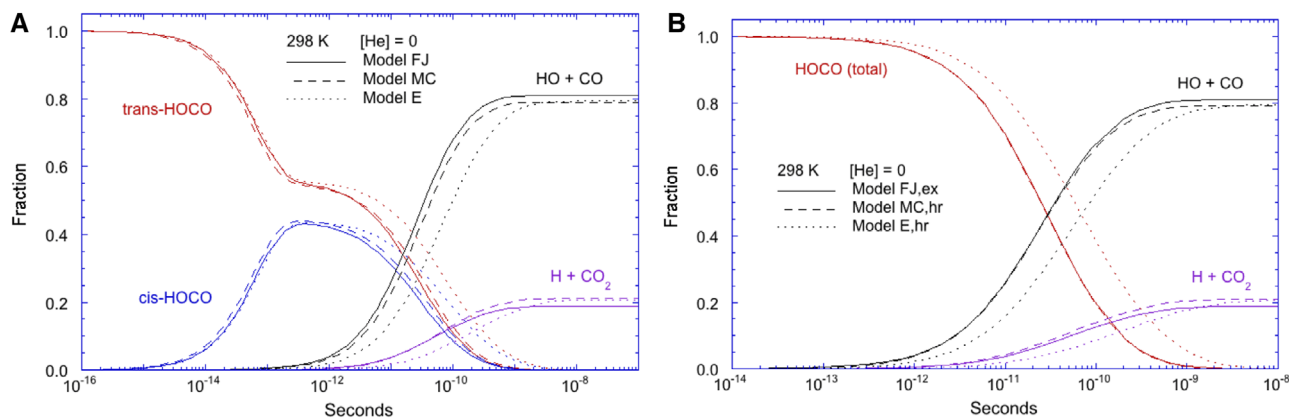


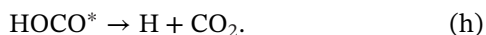
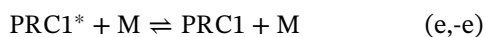
FIGURE 4 Model comparisons at 298 K and zero-pressure (HEAT thermochemistry). (A) Explicit models. (B) Hindered-rotor models compared to explicit FJ,ex. The results are color coded to denote the chemical species and the lines are solid, broken, and dotted to designate the three models [Color figure can be viewed at wileyonlinelibrary.com]

and CO is given by

$$k_z = \frac{k_a k_b}{k_{-a} + k_b}. \quad (5)$$

Equation (5) shows that a finite rate constant, k_z , exists at $[M] = 0$ because rate constant k_a is attenuated by the competition between Reactions (–a) and (b). At $[M] = \infty$, Equation (4) reduces to $k_\infty = k_a$. For this mechanism, the capture rate constant, $k_{\text{cap}} = k_\infty$.

Consider the possible role of prereactive complex PRC1. A number of researchers have described how a weakly bound PRC in the entrance channel prior to an emergent energy barrier can produce dramatic increases in bimolecular rate constants at very low temperatures.^{34,99,100} In this model, the bimolecular reactants first produce the PRC, which then undergoes quantum mechanical tunneling through the base of an energy barrier to produce products. To determine whether this mechanism is important in the HOCO reaction system at $T \gtrsim 100$ K, calculations were performed with a model that explicitly includes PRC1 and treats HOCO as a hindered rotor (ie, Model E,hr, modified to include PRC1), as follows:



The reverse of Reaction (g) is neglected here because it is very slow compared to the other reactions controlling $[\text{HOCO}^*]$ at low temperature. By using the differential equation for $d[\text{OH}]/dt$ and assuming that pseudo-steady states exist for PRC1, PRC1*, and HOCO*, followed by algebraic manipulation, an approximation for the rate constant for loss of OH (and CO) is obtained at the zero-pressure limit:

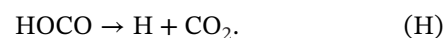
$$k_z = k_d \left(\frac{\xi}{k_{-d} + \xi} \right), \quad (6)$$

where

$$\xi = \frac{k_f k_h}{k_{-f} + k_h}. \quad (7)$$

Equation (6) is only qualitatively useful, because the rate constants in the above mechanisms are microcanonical and must be appropriately averaged over energy distribution functions, while taking into account collisional activa-

tion and deactivation. That task is performed by the master equation. At the high-pressure limit, the energy distributions of all species are canonical (ie, thermal), being maintained by collisional activation and deactivation. Thus, at the high-pressure limit the above mechanism reduces to *thermal* reactions with thermal rate constants equal to the high-pressure limit for each corresponding reaction:



At low temperatures, Reactions (–F) and (H) are slow and can be neglected to a good approximation, since the HOCO well depth is $\gg k_B T$, but rate constant k_{-D} is expected to be significant, because the dissociation energy, D_0 , for PRC1 is only a few $k_B T$, even at 100 K. In other words, once HOCO is formed, its backreaction to regenerate PRC1 is negligible and the rate constant for consumption of OH and CO can be obtained from a pseudo-steady-state analysis by setting $d[\text{PRC1}]/dt \approx 0$. This produces an expression for the high-pressure limit rate constant for loss of OH radical and CO when PRC1 is included in the mechanism:

$$k_{P\infty} = k_D \left(\frac{k_F}{k_{-D} + k_F} \right). \quad (8)$$

Equation (8) for $k_{P\infty}$ is formally similar to Equation (6) for k_z , but the relevant energy distributions are much different. The energy distribution relevant for k_z is the nascent chemical activation distribution, which is high in energy, while that for k_∞ in Equation (8) is the canonical distribution, which is low in energy. Although not of dependable quantitative accuracy, Equation (8) shows that the rate constant for net loss of OH is controlled by the branching competition between thermal Reactions (–D) and (F). Note the important distinction between the capture rate constant, $k_{\text{cap}} = k_D$, and the infinite pressure rate constant for loss of OH radical. This distinction is not important when neglecting PRC1, but it is quite important over the temperature range where k_{-D} is comparable to k_F .

In the following, we first report calculations that ignore the existence of PRC1, as in Papers I and II, and then we discuss the effects of PRC1.

4.1 | PRC1 ignored

4.1.1 | Reaction overview

Now we consider the reaction (ignoring PRC1) in more detail. Reaction is initiated when a hydroxyl radical

interacts with a carbon monoxide molecule. Capture occurs when the reaction proceeds over transition state TS1 and produces highly excited *trans*-HOCO. If the latter is not deactivated by collisions, the reaction can be reversed, or it can continue by fast, reversible formation of highly excited *cis*-HOCO via TS4. Since transition state TS2 is higher in energy than TS1, most of the excited *cis*-HOCO is produced at energies below that of TS2 barrier, thus requiring quantum mechanical tunneling to proceed to separated H + CO₂ products. The reaction also proceeds by quantum mechanical tunneling through TS3, which is associated with a very high barrier, but this pathway is of negligible importance, except at $T > 2000$ K. Throughout the progress of reaction, collisional energy transfer is occurring in competition with the reactive steps, which explains why a master equation is needed for accurate simulations.

The sequence of events described in the previous paragraph is seen in quantitative detail from the master equation simulation displayed in Figure 3, which was calculated using Model FJ,ex (ie, the fixed-J treatment of angular momentum and explicit treatment of *cis*- and *trans*-HOCO). The simulation was initiated with *trans*-HOCO distributed in the nascent chemical activation energy distribution produced by the capture of OH by CO at 298 K. This initial energy distribution is altered by the cumulative effects of collisions and chemical reaction. During the first ~ 0.2 ps, *trans/cis* equilibration of highly excited HOCO occurs under essentially collision-free conditions. The regeneration of HO + CO and dissociation to H + CO₂ occur much more slowly, gradually terminating as the excited HOCO reacts away and/or is collisionally thermalized. During the final collisional thermalization (after ~ 400 collisions in this example), the total yield of HOCO (the sum of *cis*- and *trans*-HOCO) remains essentially unchanged while the thermal *trans/cis* equilibrium ratio of ~ 12.5 is gradually established.

At 298 K, the back reaction to regenerate OH + CO and the reaction producing H + CO₂ are essentially complete before 100 collisions (or $\sim 10^{-8}$ s) have occurred and long after intramolecular vibrational energy redistribution (IVR) is expected to be complete. At higher temperatures, this process requires more collisions. At all temperatures investigated in Paper II, we found that the total yields of HOCO, H + CO₂, and HO + CO had always reached their asymptotic limits by the time that 600 collisions had occurred, t_{600} , although a minor correction had to be applied at the highest temperatures to account for the very rapid unimolecular dissociation of thermalized HOCO. However, it is clear from Figure 2 that the *trans/cis* ratio does not reach its equilibrium value until after nearly 10^5 collisions have occurred. This illustrates the very wide range of timescales important in this system.

In the OD + CO experiments reported by Bui et al,^{30,37} the *trans/cis* ratio at the end of the experiments was 5 ± 2 , which is considerably smaller than predicted based both on ATcT experimental data and on HEAT calculations (14.2 for DO+CO). Bui et al discussed this discrepancy and speculated that it may be due to errors in the theoretical IR absorption coefficients. Considering the long timescale for *trans/cis* equilibration in Figure 3, it seems quite possible that equilibration was not yet complete in the DO + CO experiments.

It is thought that collision-free IVR usually requires at least 0.1 ps and, in some cases, more than 1 ns.^{101,102} IVR timescales depend on several molecular considerations,^{101,103} including whether an excited molecule contains an internal rotor (often producing faster IVR) and whether an energy threshold for fast IVR is exceeded, which is thought to be at the energy where the density of states is greater than 10 to 100 cm⁻¹.¹⁰⁴⁻¹⁰⁷ Aside, perhaps, for PRC1 and its associated transition states, the HOCO system seems to satisfy the requirements for relatively fast IVR, and we are not aware that any dynamics studies have reported significant effects due to slow IVR in this system. A possible exception is IVR in prereactive complexes,¹⁰⁸ such as PRC1, where the very low-frequency noncovalent vibrations do not couple strongly to the much higher frequency covalent modes associated with covalent bonding, thus slowing the rate of IVR. For covalently bound HOCO, we expect that limitations due to IVR may affect the results at $t < 10$ ps in the absence of collisions. When collisions are important, collision-induced IVR may accelerate energy randomization, but we have no way of estimating its magnitude.

4.1.2 | High- and zero-pressure limits

The rate constants $k_z(T)$ and $k_\infty(T)$ can be calculated using no adjustable parameters, and the Fixed-J treatment of angular momentum is exact at both limits, thus a comparison between theory and experiment for this ab initio model is an important test. Calculated values of the theoretical $k_\infty(T)$ and $k_z(T)$ are summarized in Table S1 in the Supporting Information.

Because the Fixed-J model (Model FJ) is exact in the absence of collisional energy transfer, we can assess the accuracy of the model based on Marcus' centrifugal corrections (Model MC) and the one based solely on total energy (Model E) by comparing them to Model FJ at $[M] = 0$, as shown in Figure 5. All of the simulations were initiated at $t = 0$ with *trans*-HOCO in the chemical activation energy distribution formed by the reaction of OH with CO. The *cis-trans* equilibration ($t < 0.5$ ps), which is much more rapid than the other reactions, is reproduced with good accuracy

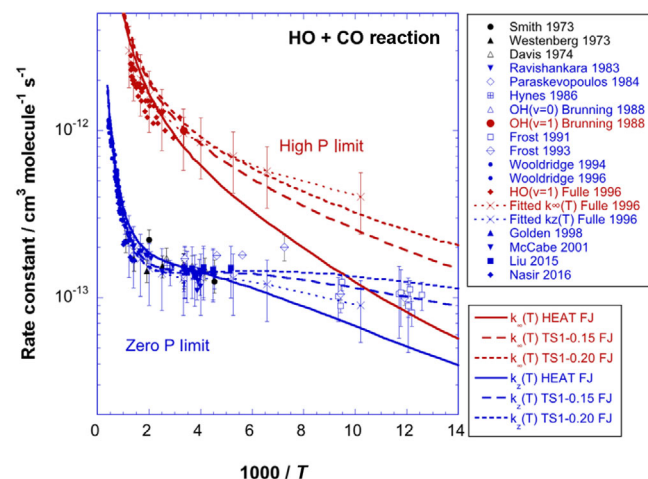


FIGURE 5 Limiting rate constants $k_z(T)$ and $k_\infty(T)$ for OH + CO. Experimental data for near-zero and near-infinite pressures are shown as symbols. The solid lines are ab initio predictions using HEAT-345 thermochemistry and the Fixed-J treatment of angular momentum. The thick broken lines are for two empirical models with adjusted thermochemistry, as described in the text [Color figure can be viewed at [wileyonlinelibrary.com](#)]

by both approximate methods, but differences emerge during the subsequent dissociation reactions that produce the two sets of final products ($t > 0.5$ ps). Model MC is in very good agreement with the exact results over the entire time span, while Model E is somewhat less accurate, because it predicts slower decomposition rates. Because the cis-trans equilibration is faster than any other process in the explicit models, the hindered rotor approximation produces excellent agreement with the corresponding explicit models, while producing a 200 \times speedup of the computer simulations.

In Model MC, the reaction threshold energies are lowered due to the centrifugal corrections, which depend on the moments of inertia of the reactants and transition states. The moments of inertia of TS4 for cis-trans isomerization and TS2 for dissociation are almost the same as those of the two HOCO isomers. Thus, the centrifugal corrections for reactions via those transition states are minimal and the rates predicted by Model MC are almost the same as those predicted by Models FJ and E. However, because the moment of inertia of TS1 is about twice as large as that for *trans*-HOCO, the critical energy is lowered, thus increasing the reaction rate via TS1, in agreement with the Model FJ. Model E lacks this correction and thus predicts a rate constant that is too slow. In general, the models with angular momentum corrections predict faster rate constants than those without such corrections.

In the covalent OH + CO reaction system, all of the transition states are tight and thus the centrifugal effects are relatively small. Nonetheless, Model MC is distinctly more

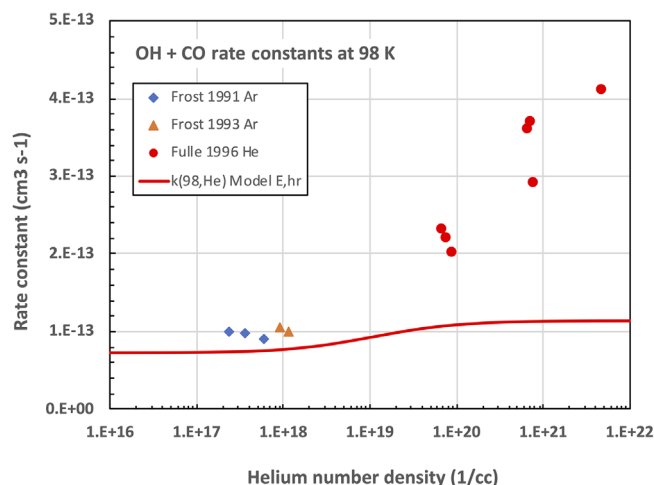


FIGURE 6 OH + CO rate constants near 98 K. Experimental data^{54,110,111} are shown as points and the theoretical rate constants (obtained using Model E,hr with ab initio HEAT thermochemistry and $\alpha_{\text{HOCO}} = 150 \text{ cm}^{-1}$) are shown as the solid line [Color figure can be viewed at [wileyonlinelibrary.com](#)]

accurate than Model E, but neither is as accurate as Model FJ, which is theoretically exact at the zero-pressure limit.

As shown in Figure 5, $k_\infty(T)$ and $k_z(T)$ predicted for OH + CO from HEAT-345Q thermochemistry are in very good agreement with the near-infinite and near-zero pressure experimental data at temperatures above ~ 300 K. At temperatures below ~ 300 K, the ab initio $k_\infty(T)$ falls below the experimental data and this discrepancy grows systematically as the temperature is lowered. The experimental $k_\infty(T)$ (with 2σ errors of $\pm 40\%$) near 100 K is 4 times as large as the predicted values (see Figure 6). As the temperature is increased, the discrepancy between theoretical and experimental values decreases until it is approximately equal to the 2σ error at ~ 200 K and less than the 1σ error at ~ 300 K (see Figure 2). At higher temperatures, discrepancies between theory and experiment are not apparent, possibly in part because the experimental pressures are not high enough to reach near k_∞ .

The predicted $k_z(T)$ is higher than the experimental rate constants reported by Ravishankara and Thompson¹⁰⁹ at low pressures, but is in very good agreement with subsequent experiments from the same group.⁶² The predictions are also in very good agreement with the experiments of Golden et al⁶¹ and Liu and Sander.⁶⁰ At temperatures lower than 250 K, $k_z(T)$ is somewhat lower than the experiments of Frost et al,^{110,111} but the agreement is still quite good.

4.1.3 | Empirical tests: Energy and tunneling adjustments

To determine whether adjustments to the thermochemistry or the tunneling treatment might account for the

discrepancies that are apparent at low temperatures, empirical adjustments were investigated. Two transition states are responsible for determining $k_z(T)$ and $k_\infty(T)$. To increase the theoretical $k_\infty(T)$, the energy of the TS1 barrier can be reduced, or the rate of tunneling can be increased by increasing the imaginary frequency, but such changes are found to simultaneously increase the predicted $k_z(T)$. To compensate for increases in $k_z(T)$, the energy of TS2 can be increased, or tunneling through the TS2 barrier can be reduced artificially.

In the first empirical model (designated TS1-0.15), the electronic energy of TS1 was adjusted downward by $-0.15 \text{ kcal mol}^{-1}$ and TS2 was adjusted upward by $+0.3 \text{ kcal mol}^{-1}$. The results are summarized in Table S2 in the Supporting Information. With these adjustments, the predicted $k_\infty(100 \text{ K})$ matches the lower 2σ error bar of the experimental data of FHHT, while simultaneously matching $k_z(300 \text{ K})$, as shown in Figure 8.

In the second empirical model (designated TS1-0.20), the electronic energy of TS1 was adjusted downward by $-0.20 \text{ kcal mol}^{-1}$ and TS2 was adjusted upward by $+0.4 \text{ kcal mol}^{-1}$. The results are summarized in Table S3 in the Supporting Information. With these adjustments, the predicted $k_\infty(100 \text{ K})$ matches the lower 1σ error bar of the experimental data of FHHT, while simultaneously matching $k_z(300 \text{ K})$ (see Figure 8). We also determined that for theory to match the experimental $k_\infty(100 \text{ K})$, the electronic energy of TS1 would have to be lowered by $-0.23 \text{ kcal mol}^{-1}$, but we did not pursue this case any further.

For consistency, any adjustments made to the electronic energy in the OH + CO system must also be applied to the OD + CO isotopologue. Three models for electronic energy (HEAT, TS-0.15, and TS-0.20) were investigated for the deuterated reaction OD + CO, and the results are shown in Figure 5. Here, the experimental data are much more limited. The sole experimental value of $k_\infty^D(T)$ was obtained by measuring the deactivation of OD ($v = 1$). Agreement between experiment and HEAT theory is excellent; the empirical adjustments degrade the agreement slightly. The experimental data for $k_z^D(T)$ were obtained by extrapolating pressure-dependent rate constants for OD ($v = 0$) + CO measured in various bath gases to $[M] = 0$. Here, without adjustments, the computed $k_z^D(300)$ is $\sim 30\%$ lower than the centroid of the experimental data around 300 K and the agreement becomes distinctly worse as the empirical energy adjustments are applied. We conclude from these calculations that empirical energy adjustments to TS1 (and TS2) do not improve the theoretical description of the combined OH + CO and OD + CO experimental data. The $\sim 30\%$ discrepancy in $k_z^D(300)$ between ab initio theory and the OD + CO experiments possibly suggests that the predicted TS2 barrier height may be too high by perhaps $\sim 0.1 \text{ kcal mol}^{-1}$.

A second empirical test was performed by arbitrarily varying the imaginary frequency associated with TS1, leaving all other parameters untouched. It was found that this procedure could produce excellent agreement with $k_\infty(T)$ measured by FHHT, as shown in Figure 6, but the imaginary frequency had to be increased from 221 to 600 cm^{-1} . This enormous adjustment is simply unacceptable. Generally speaking, even low-level quantum chemistry methods can predict harmonic frequencies (including the imaginary frequency) that are accurate to within perhaps 10–20%^{112–114} and the present level of theory is usually accurate to within perhaps 20 cm^{-1} .¹¹⁵ Thus, an error of almost $\times 3$ in the imaginary frequency is not credible. Furthermore, as the imaginary frequency is increased, the predicted $k_z(T)$ is found to diverge strongly from the experimental values reported by FHHT, as shown in Figure 5.

It is possible that some combination of energy and tunneling adjustments can bring the predicted $k_\infty(T)$ and $k_z(T)$ into agreement with the experiments, but it is not at all clear that such a curve-fitting exercise can simultaneously fit the experimental H/D kinetic isotope effects satisfactorily. Furthermore, the required energy adjustments are only marginally consistent with the known error bounds of the HEAT protocol. Thus, we conclude that these empirically adjusted models are not superior to the ab initio calculations. We also observe that the experimental data for the OD + CO system show considerable scatter and the stated experimental errors have probably been underestimated.

4.1.4 | Intermediate pressures

In the OH + CO reaction system that neglects PRC1, all of the transition states are tight and thus the centrifugal effects are relatively small. Nonetheless, angular momentum treatments have an important impact on the energy transfer parameters that are adjusted to fit experimental reaction rate data. Since collisional energy transfer is in competition with chemical reaction, underestimated reaction rate constants in this system will result in underestimated collisional energy transfer rates and vice versa.

Because the angular momentum treatments described in this paper are approximations and the energy transfer parameter α is not known, α was adjusted empirically to match experimental total rate constants reported in the literature. Fitting of data can be achieved in several ways. For simplicity in the present work, we have fitted a single “target” rate constant $k_{\text{tar}}(T, [\text{He}]_{\text{tar}})$ where $[\text{He}]_{\text{tar}}$ is the helium number density at which the experimental $k_{\text{tar}}(T, [\text{He}]_{\text{tar}}) \approx k_\infty(T)/2$. Note that a relatively wide range of α values can provide adequate fits to a dataset at any one temperature. Fitting a specific target value, which may not

TABLE 2 OH + CO target rate constants^a

T	[He]	$k_{\text{tar}}(T, \text{He})$
98	6.9E+20	3.40E-13
190	3.9E+20	4.60E-13
250	1.5E+20	3.90E-13
298	2.0E+20	4.11E-13
400	2.6E+20	4.20E-13
500	1.0E+21	6.00E-13
819	3.6E+21	8.60E-13

^aUnits: [He] / molecules cm⁻³, $k_{\text{tar}}(T, \text{He})$ / cm³ molecule⁻¹ s⁻¹.

be truly representative of the entire set, is not be the best choice for a global fit, but that is not the goal of the present work. The goal of the present work is to confined to identifying the strengths and weaknesses in theory and experiment. The targets and resulting fitted values of $\alpha(T)$ for each ab initio ME model are reported in Tables 2 and 3, respectively. At some temperatures, entries are missing in Table 3 because the computed $k_{\infty}(T)$ is smaller than the experimental $k_{\text{tar}}(T, \text{He})$, thus making it impossible to fit the targets.

The fitted parameters in Table 3 show that the three treatments of angular momentum require distinctly different values of α to fit the targets, but it should be emphasized that a relatively wide range of α can provide a tolerable description of the entire experimental dataset at each of the lower temperatures, as illustrated for 298 K in Figure 9. This is because the high-pressure limit suggested by the experiments at 298 K is ~20% higher than predicted by theory, and there are also differences at the zero-pressure limit, thus affecting the shapes of the curves and the fitted value of α . At higher temperatures, the fitted values of α are better defined, because the theoretical $k_{\infty}(T)$ and falloff curves are in close agreement with the experiments (Figure 10). At lower temperatures (Figures 6 and 10), there exists a marked discrepancy, which is an important motivation for the present work and is discussed below.

As noted above, the models based on E refer to total energy alone and thus the parameter α refers to the transfer of total energy. In models based on FJ and MC, however, α refers to transfer of active energy, ϵ . It is also apparent in Table 3 that α depends on temperature and $\alpha(T)$ often increases as T is lowered. This inverse temperature dependence is most pronounced for the models based on treatments FJ and MC. Energy transfer measurements in nonreactive systems predict little or no temperature dependence and energy transfer parameters derived from master equation simulations of other reaction systems tend to predict that $\alpha(T)$ is proportional to T^{α} , where the exponent is $\lesssim 1$. The inverse dependence on T is uncommon but not unique, and we surmise here that it is at least partly due to the fact that the experimental high-pressure limit is significantly higher than the theoretical $k_{\infty}(T)$ and small differences between theory and experiment are apparent in $k_z(T)$ at temperatures ≤ 300 K. The difference in magnitude of $k_{\infty}(T)$ is ~20% at 300 K and grows to approximately a factor of ~4 at 100 K. In order to compensate for this discrepancy, the fitted value of $\alpha(T)$ must increase.

The relative performance of the three angular momentum treatments can be assessed by comparing the models with experiments at ~298 K (Figure 2). All three models treat *cis*- and *trans*-HOCO explicitly, utilize the “ab initio” HEAT thermochemistry, and use the respective values of α presented in Table 3(A). The three models are in excellent agreement with the experimental data, which have 2σ uncertainties of ~40% (not shown) at high pressures. Near the zero-pressure limit, all three models perform well, but Model FJ,ex performs the best. At the highest pressures, the measured rate constants are larger than the theoretical $k_{\infty}(298)$, which is the same for all three models and which is about 20% lower than the empirical fit reported by FHHT (see Figure 6). It is interesting to note that the approach to the high-pressure limit predicted by the calculations mimics the subtle curvature that is apparent in the data of FHHT at very high pressure, despite the

TABLE 3 Energy transfer parameters^a (α) fitted to targets^b for five ab initio^c ME models

T	FJ,ex	MC,ex	E,ex	MC,hr	E,hr
98	–	–	–	–	–
190	–	–	–	–	–
250	510	352	167	305	148
298	320	234	138	267	149
400	225	184	129	203	139
500	188	159	125	170	138
819	215	160	154	175	165

^aUnits α/cm^{-1} ; uncertainty $\approx \pm 5\%$.

^bSee Table 1.

^cHEAT-345Q thermochemistry, without any adjustments.

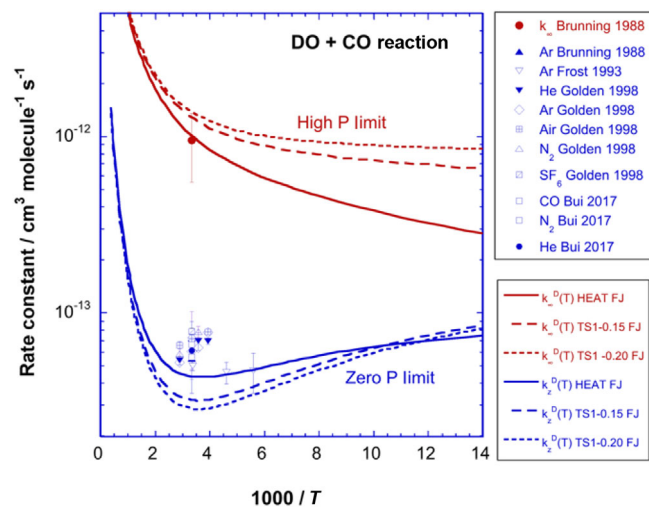


FIGURE 7 Limiting rate constants $k_z^D(T)$ and $k_{\infty}^D(T)$ for OD + CO. Experimental data for near-zero and near-infinite pressures are shown as symbols. The solid lines are ab initio predictions using HEAT-345 thermochemistry; broken lines are for two empirical models with adjusted thermochemistry, as described in the text. All of these theoretical calculations were performed using the Fixed-J treatment of angular momentum [Color figure can be viewed at wileyonlinelibrary.com]

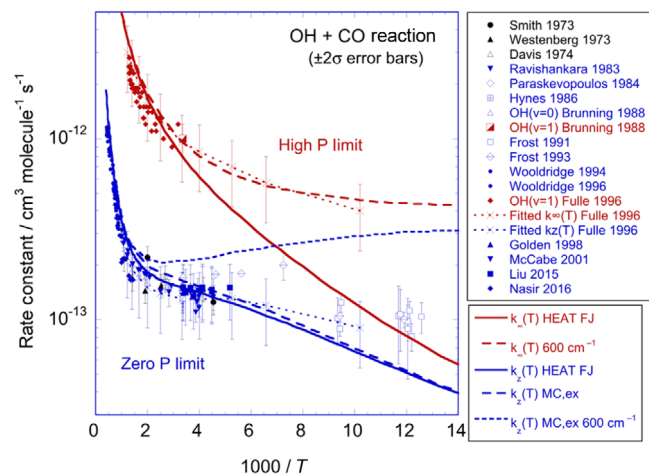


FIGURE 8 Predicted rate constants (compared to experimental data) with and without changing the imaginary frequency from 221 to 600 cm^{-1} [Color figure can be viewed at wileyonlinelibrary.com]

large reported 2σ experimental uncertainties (Figure 7). This curvature is also apparent in the experimental data at lower temperatures, as shown in Figure 10, which compares experiment and calculations over a wide range of temperatures.

Calculations were also performed using the empirical energy adjustments described above. Because these adjusted models do not perform well in describing the H/D kinetic isotope effects, they are not recommended, but the

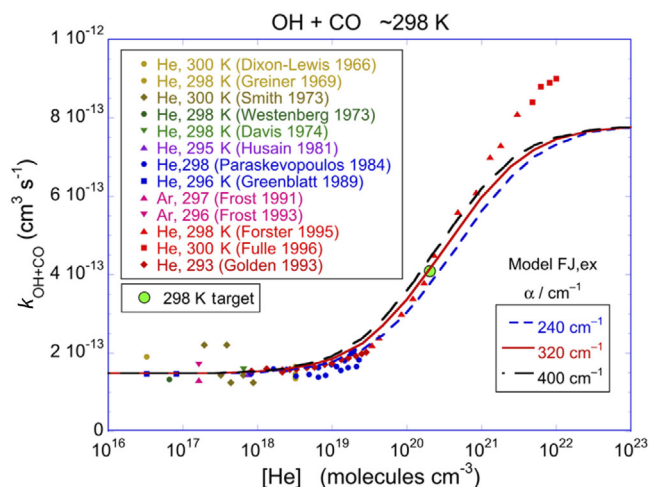


FIGURE 9 Dependence of theoretical results on $\alpha(298)$. Note that the experimental 2σ uncertainties are $\pm 40\%$ at high pressures [Color figure can be viewed at wileyonlinelibrary.com]

fitted values of α listed in Tables S4 (in the Supporting Information) illustrate the same points made earlier. The different treatments of angular momentum require different values of α to fit the targets. Moreover, the adjustments to the thermochemistry also affect the fitted values and predicted temperature dependence.

4.1.5 | OD + CO reaction

Calculations were performed using the FJ,ex, E,ex, and MC,ex models for the deuterated reaction in the same ways as described for OH + CO. The thermochemistry for OD + CO is based on using the experimental OH spin-orbit constant (A_{SO}) for OD radical, since the A_{SO} mass-dependence is negligible. Because of the rotational constant of OD is smaller than that of OH, the HVV treatment predicts that the spin-orbit stabilization energy in OD is greater (52.5 cm^{-1} vs 38.2 cm^{-1}). The OD + CO thermochemistry is listed in Table 1.

The results obtained using the FJ,ex model at zero and infinite pressure are presented above in Figure 7. At intermediate pressures, results obtained using the FJ,ex model with ab initio HEAT thermochemistry predict that the rate of production of *trans*-DOCOC is 2.0 \times the rate of production of *cis*-DOCOC at 298 K and He pressures ranging from 0.1 to $> 10^4$ Torr, in excellent agreement with the experiments of Bui et al.³⁰ However, the calculated equilibrium *trans*/*cis* ratio at 298 K of 14.2 is higher than the experimental ratio of 5 ± 2 reported by Bui et al.³⁰ As discussed above, this discrepancy may be due to a combination of nonequilibrium effects and errors in calculated IR absorption coefficients.

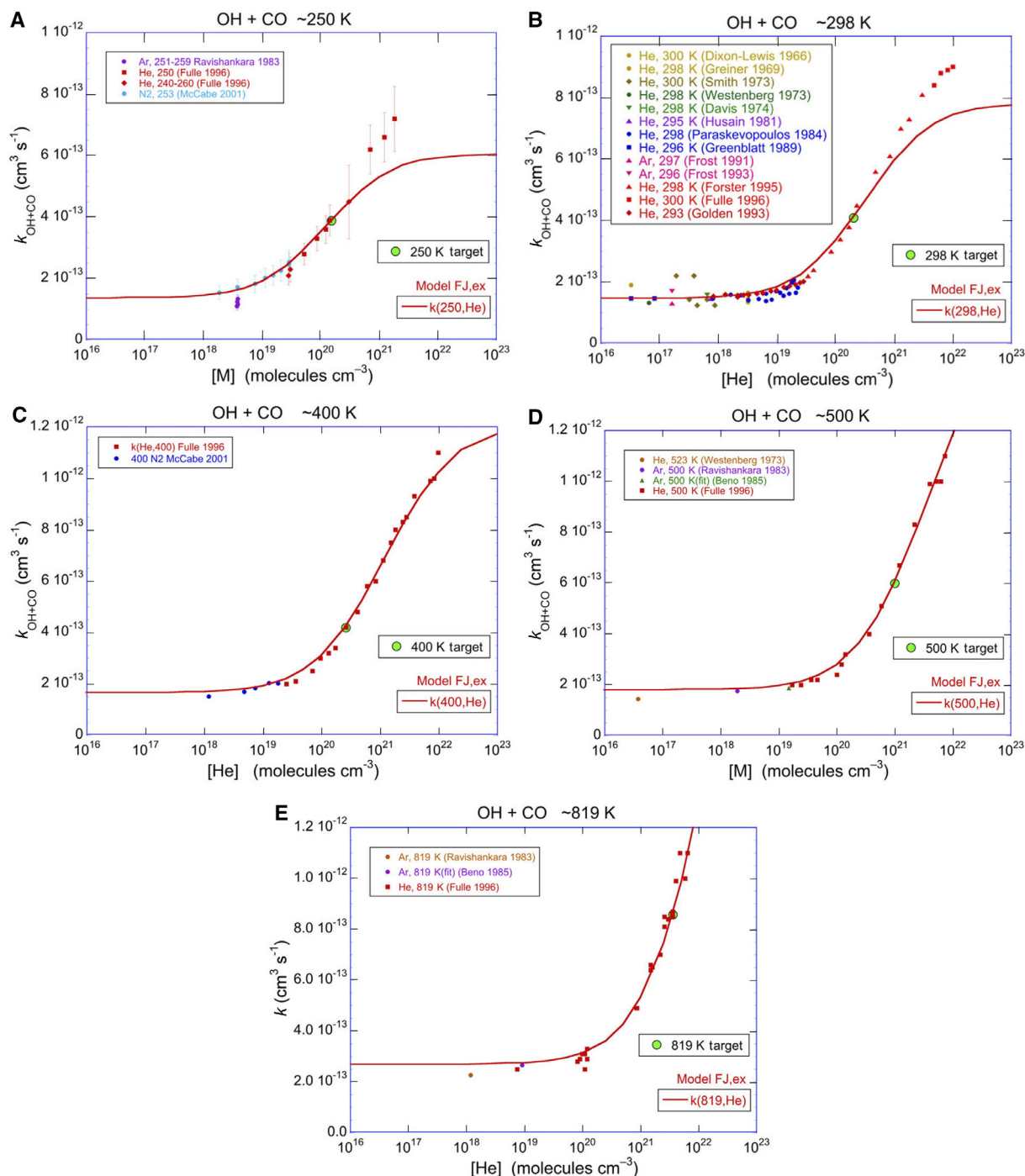


FIGURE 10 Experiments (points) and simulations (lines) using Model FJ,ex at temperatures from ~ 250 to ~ 819 K. Targets (Table 1) are shown as green circles. All simulations were performed using the “ab initio” HEAT-345Q thermochemistry. (For energy transfer parameters, see Table 2) [Color figure can be viewed at wileyonlinelibrary.com]

4.2 | PRC1 included

4.2.1 | Enhanced rate constants from including PRC1?

Because the capture rate constant is equal to the ab initio k_{∞} for TS1 in the simulations that ignored the exist-

ence of PRC1, and k_{∞} is lower than the measured high-pressure limit at low temperatures, it was not possible to match the experiments without making adjustments (and the adjustments turned out to be unacceptable). However, when PRC1 is included (see Figure 11), k_{cap} becomes much larger, because it is based on k_{∞} for TSO, a loose transition state, instead of the much smaller k_{∞} for TS1,

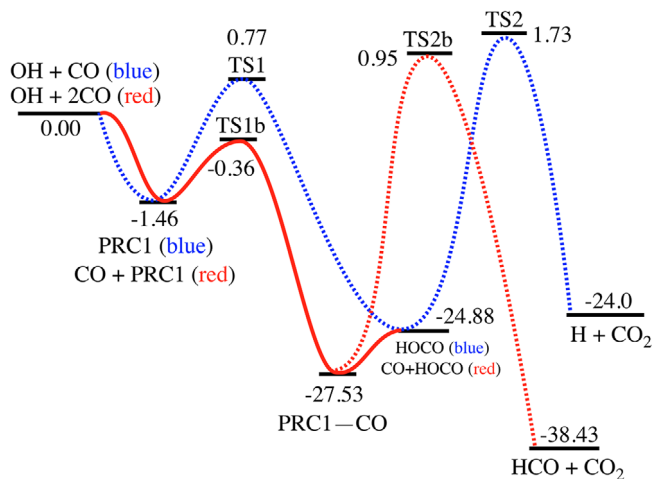


FIGURE 11 PES showing reactions between CO and PRC1. Relative energies (kcal mol^{-1} , including zero-point energy) were calculated as described in the text [Color figure can be viewed at wileyonlinelibrary.com]

a tight transition state (see Table S6 in the Supporting Information). This suggests that the high-pressure limit for the mechanism including PRC1 might be large enough to match or exceed the experimental high-pressure limit. To explore this possibility, we performed simulations using Model E,hr, augmented by including PRC1. We also investigated the possibility that bimolecular reactions involving PRC1 might play a role in the experiments. Simulations were performed over a range of temperatures encompassing 98 K, where the discrepancy between theory and experiment is greatest. All simulations were performed using the capture rate constant, k_{cap} , obtained by using J-resolved microcanonical VTST, based on constrained optimizations at OH–CO bond distances ranging from 2.4 to 10 Å. In addition, canonical VTST calculations performed over a wide range of temperatures showed that the canonical variational transition state is located at ~ 4.0 Å for $T = 98$ K and 2.4 Å for all temperatures ≥ 200 K. Because the variational TSs at 2.4 Å are at the end of the bond distance range, k_{cap} is probably of reduced accuracy for $T \gtrsim 200$ K.

Simulations were performed for rate constants k_z and $k_{P\infty}$. The former was obtained from the master equation simulations and the latter from Equation (8) with thermal rate constants obtained from the simulations. Both were calculated by using the HEAT thermochemistry without adjustments ($D_0 = 581 \text{ cm}^{-1}$) and by adjusting the PRC1 dissociation energy to match the upper limit $D_0 = 410 \text{ cm}^{-1}$ reported by Pond and Lester.⁷⁴ Simulations at other assumed values of D_0 were also performed. As described above, the HEAT thermochemistry is based on assuming that the spin-orbit constant, A_{SO} , for PRC1 is the same as that for the OH radical. The results of the simula-

tions are displayed in Figures S3, S4, and S5 and Table S6 in the Supporting Information.

Results of thermal reaction simulations as functions of He pressure and assumed values of α_{PRC1} are presented in Figure S3 in the Supporting Information, which shows that the thermal unimolecular reaction of PRC1 at low pressures is near the low-pressure limit. The rate constant is approximately proportional to both $[\text{He}]$ and to α_{PRC1} and can be expressed as $k_{\text{uni}}(98) \approx 10^{-14} \alpha_{\text{PRC1}} [\text{He}] \text{ s}^{-1}$. At all temperatures, $k_z(T)$ was computed according to Equation (8), using results from master equation simulations and canonical rate constants computed from the sums and densities of states by the MULTIWELL master equation code and the equilibrium constant computed by THERMO. The rate constants computed with and without PRC1 are essentially identical, as shown in Figure S4 in the Supporting Information. This figure also shows that the results obtained using D_0 from Pond and Lester are essentially identical to those obtained by using D_0 from HEAT calculations.

The zero-pressure rate constant for OH + CO at $P = 0$ and 98 K is predicted by HEAT (including PRC1) to be $k_z(98) = 8.1 \times 10^{-14} \text{ cm}^3 \text{ molecule}^{-1} \text{ s}^{-1}$, which is in very good agreement with the experimental data and $\sim 11\%$ higher than the rate constant predicted when ignoring PRC1 ($7.3 \times 10^{-14} \text{ cm}^3 \text{ molecule}^{-1} \text{ s}^{-1}$ for the E,hr model). This difference is probably due to small changes in quantum mechanical tunneling and to the difference between the initial chemical activation energy distributions near the top of the TS1 energy barrier. Because the energy distribution controls the competition between regeneration of OH + CO and isomerization to produce excited HOCO, it affects the value of $k_z(T)$. In both cases, with and without including PRC1, tunneling through the TS1 barrier to produce HOCO also makes a contribution. At the high-pressure limit, the results predict that $k_{P\infty}(98) = 1.26 \times 10^{-13} \text{ cm}^3 \text{ molecule}^{-1} \text{ s}^{-1}$, which is almost identical to the value obtained when ignoring PRC1 ($k_{\infty}(98 \text{ K}) = 1.13 \times 10^{-13} \text{ cm}^3 \text{ molecule}^{-1} \text{ s}^{-1}$). Thus, we conclude that simply including PRC1 in the mechanism does not lead to improved agreement with the low-temperature data from FFHT.

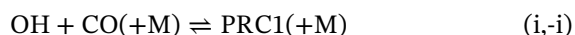
4.2.2 | Bimolecular reactions involving PRC1?

Another possible explanation for the discrepancy between the experimental and theoretical values of $k_{\infty}(98)$ is that PRC1 might undergo rapid bimolecular reaction, thus preventing regeneration of OH + CO and resulting in the larger rate constant reported by FHHT. At 98 K, the gas mixtures used by FHHT contained He, CO, CH_4 , and O_3 .

In principle, PRC1 can react with all of these species, except for He.

Bimolecular reaction of PRC1 with O₃ is expected to be negligible, because the partial pressure of O₃ in the mixture at 98 K was < 1 mbar and to be important, the required rate constant would have to be unphysically large. The partial pressure of CH₄ was 10–20 mbar (ie, ~10¹⁸ molecules cm⁻³ at 15 mbar) and if the reaction PRC1 + CH₄ has the same rate constant as OH + CH₄ (~3 × 10⁻²⁰ cm³ s⁻¹ at 98 K),³ then the time constant for the bimolecular reaction will be several orders of magnitude too slow to be important.

The last remaining candidate for the bimolecular reaction with PRC1 at 98 K is the 30–90 mbar partial pressure of carbon monoxide (~3.7 × 10¹⁸ cm⁻³ at 50 mbar) present in the gas mixtures. The PES for this reaction is depicted schematically in Figure 11. As shown in the Supporting Information, PRC1 is produced and destroyed via Reactions (i) and (-i), and the latter competes with Reaction (j):



The vibrationally excited OCHOCO* intermediate is a weakly bound hydrogen-bonded complex, which is expected to dissociate extremely rapidly, just as in the radical complex (ie, chaperon) mechanism familiar from collisional energy transfer studies.^{116–119} The net result of this reaction is to catalyze formation of HOCO and prevent regeneration of OH + CO, thus enhancing the net rate of loss of OH. The PES and properties of the intermediate are depicted in Figure 10 and Table S5 in the Supporting Information, based on calculations using the mHEAT-345(Q) method.

In the pressure falloff regime, a pseudo-steady-state analysis based on Reactions (i, -i) and Reaction (j) (see Supporting Information) produces the following expression for k_{OH} , the pseudo-first-order total rate constant for loss of OH:

$$k_{\text{OH}} = \frac{k_i k_j [\text{CO}]}{k_{-i} + k_j [\text{CO}]} \quad (10)$$

At 98 K and [He]_{target} rate constants k_i and k_{-i} are ~6 × 10⁻¹² cm³ s⁻¹ and ~6 × 10⁸ s⁻¹, respectively. Thermal rate constant k_j was calculated using SCTST based on the molecular parameters in Table S5 in the Supporting Information, giving $k_j(98) = 2.3 \times 10^{-14}$ cm³ s⁻¹. With these parameters, Equation (10) predicts that $k_{\text{OH}} \approx 8 \times 10^{-16}$ cm³ s⁻¹, which is ~500 times smaller than the rate constant reported by FHHT. To approach the magnitude of the experimental rate constant, the energy barrier for Reaction (j) would need to be almost negligible.

5 | SUMMARY AND CONCLUSIONS

The present work was motivated by the observation that master equation simulations using ab initio HEAT thermochemistry and SCTST rate constants are in very good to excellent agreement with measurements of $k_z(T)$ for HO + CO at both high and moderate-to-low temperatures and with measurements of $k_\infty(T)$ at $T \geq 250$ K, but not at lower temperatures.^{18,19} Why is the agreement not even better? Based on past experience, the most obvious hypothesis to explain this discrepancy is that the computed thermochemistry is in error. We therefore slightly improved the HEAT thermochemistry²⁸ by using an improved calculation of the adiabatic (DBOC) correction and, more significantly, the treatment of Hill and van Vleck⁶⁵ for the coupling of rotational and electronic angular momenta to reckon the position of the OH (and OD) zero-point level relative to that obtained with a simplistic treatment of an uncoupled spin-orbit calculation. We also improved the computed partition function for OH radical by implementing the HVV treatment of spin-orbit coupling. The end result of these improvements was that their effects cancelled and the computed rate constants (and the discrepancy) remained almost unaffected. We also adjusted the electronic energies empirically to bring $k_z(T)$ and $k_\infty(T)$ into agreement with the experimental data from 100 to 820 K. This exercise was successful, but when the same adjustments were applied to the OD + CO system, the agreement with experiments became worse. Thus, we conclude that simple adjustments to the thermochemistry cannot explain the $k_\infty(T)$ discrepancy between theory and experiment at low temperature.

Quantum mechanical tunneling is important in this reaction system, and so we investigated the sensitivity to the imaginary frequency, ω_{imag} , which is a major determinant of tunneling. We found that enhancing the tunneling by increasing the magnitude of ω_{imag} for transition state TS1 could bring the theoretical rate constants into agreement with the measurements at all temperatures, but the change in magnitude (by a factor of ~3) is simply not credible. Furthermore, the increase in tunneling caused the theoretical $k_z(T)$ to shift from its former excellent agreement with measurements into very poor agreement. Thus, this empirical adjustment to tunneling is not satisfactory.

In another series of calculations using ab initio HEAT thermochemistry, we investigated the possibility that pre-reactive complex PRC1 is participating meaningfully in the kinetics at ~100 K. Microcanonical VTST rate constants for forming the complex were used along with microcanonical SCTST rate constants for all of the other reactions in master equation simulations at low temperature. Although PRC1 is formed with a large rate constant, it dissociates extremely rapidly because it is weakly bound, thus

regenerating OH radical. This process is much faster than the time resolution in the FHHT experiments at 100 K and the ab initio calculations indicate that it did not affect the measured $k_{\infty}(T)$. When the ab initio well depth is reduced by $\sim 200 \text{ cm}^{-1}$ to match the upper limit reported by Pond and Lester,⁷⁴ the influence of PRC1 should be even smaller. Thus, we conclude that simply including PRC1 in the mechanism does not improve the agreement between experiment and theory at temperatures down to $\sim 100 \text{ K}$.

Another possibility is that the regeneration of OH radical is suppressed by a fast-bimolecular reaction between PRC1 and another component in the gas mixture. To be important, the pseudo-first-order rate constant for the bimolecular reaction would have to be faster than the unimolecular reaction for decay of PRC1. At 98 K, the only component in the mixture that might plausibly react with PRC1 is CO; all of the other components react too slowly, or their concentrations are too low. According to our calculations, the bimolecular reaction would have to be barrierless; even then it might still be too slow.

It is also possible that deficiencies in the master equation calculations might contribute to the discrepancy. To address this possibility, we investigated three different treatments of angular momentum in 1D master equation codes (with SCTST rate constants) that are used as workhorses in analyzing experimental data and making predictions. In many calculations, the explicit treatment of *cis*- and *trans*-HOCO was replaced with a hindered internal rotor model, which was nearly three orders of magnitude faster computationally. Intermediate pressures were investigated by using these master equation models and values of the energy transfer parameter α (exponential model) that empirically fitted target rate constants at specified temperatures and pressures. All of these treatments were highly successful in fitting the HO + CO experimental data for $T \geq 250 \text{ K}$ and over the entire range of and pressures. Thus, the $k_{\infty}(T)$ discrepancy between theory and experiment at low temperature persisted.

A by-product of these calculations was to show clearly that each treatment of angular momentum, each version of thermochemistry (ab initio and adjusted), and each temperature requires a different empirical value of the energy transfer parameter α (exponential model) to fit the targets, as expected. Because the fitted value of α is sensitive to so many different factors, it seems unlikely that accurate values of α can be transferred from one chemical activation system (like OH + CO) to another.

We also inspected the experimental data very closely. Experimental data near the zero-pressure limit has been reported by several research groups, and all of the results for $k_z(T)$ are reasonably consistent over the entire range of temperatures. The high-pressure limit rate constant, $k_{\infty}(T)$, has been measured in two ways: extrapolation of

direct kinetics measurements in high pressures of buffer gases and measurement of the rate constant for deactivating OH($v = 1$) or OD($v = 1$) by reactive collisions with CO and then assuming that the deactivation rate constant can be identified with $k_{\infty}(T)$. Two groups have reported results from the second of these methods at $T \geq 298 \text{ K}$, and the results are quite consistent. One of the two groups, FHHT, has also reported kinetics results at extremely high pressures of helium and obtained $k_{\infty}(T)$ by extrapolation. Over the temperature range where both approaches have been used, the results agree with each other. But over the critical temperature range below 250 K, FHHT obtained $k_{\infty}(T)$ only by extrapolating results obtained at very high pressures of helium buffer gas. After close inspection, we did not find any reasons to discount the results reported by FHHT, but we surmised that the experimental errors at low temperature may have been underestimated.

Since only the one set of measurements by FHHT has been reported for pressure-dependent rate constants for OH + CO in the critical regime of very low temperature and very high pressures, we feel that it will be useful for other groups to replicate the experiments. Data for the OD + CO system are also rather sparse and somewhat scattered. Measurements of the deactivation of OH($v = 1$) and OD($v = 1$) by CO over a wide temperature range, especially below 250 K, will be very informative. And indeed, we are aware that measurements of OH($v = 1$) deactivated by CO are currently underway (Ian Sims, private communication, March 9, 2020). Greenslade et al have reported LIF detection of PRC1 in molecular beams,⁶³ and it will be useful to detect and measure its kinetics at low temperatures in bulk buffer gases, if feasible. Its detection in bulk gas would open the possibility of investigating its possible reactions with CO, O₃, etc.

Current theoretical capabilities are deficient to some degree. As electronic structure methods continue to improve, the level of accuracy (which is already much higher than it was just a handful of years ago) will continue to improve, although further improvements will necessarily increase computational cost significantly. Together with advances in computer architectures, very accurate calculations – especially for larger chemical systems such as reactions like Reaction (j) will emerge as a possibility. Our current master equation methods utilize versions of TST, which implicitly neglects the finite rate of intramolecular vibrational relaxation and other nonstatistical effects. Possibly such effects come into play in the OH + CO system at the low temperatures where prereactive complexes are important and where theory and experiment currently disagree. But the close examination of the theoretical methods in the present work gives us not only more confidence in our “ab initio” results for $k_{\infty}(T)$ and $k_z(T)$, but also gives us better understanding of the strengths and limitations

of master equation simulation methods that have been used in this work. While there is a strong probability that new experiments will simply confirm most of the results reported by FHHT, it is also possible that our understanding of the reaction system will be altered. In any event, it will be interesting to see if the magnitude of discrepancies with theory at very low temperatures persists.


ACKNOWLEDGMENTS

We thank Horst Hippler, Ian Sims, and Lan Cheng for technical discussions and for communicating unpublished information. JRB thanks the Department of Climate and Space Science & Engineering at the University of Michigan for facilities and technical support. JFS and TLN thank the U.S. Department of Energy (grant no. DE-FG02-07ER15884) and the National Science Foundation (grant no. CHE-1748821) for financial support.

ORCID

John R. Barker  <https://orcid.org/0000-0001-9248-2470>

John F. Stanton  <https://orcid.org/0000-0003-2345-9781>

Thanh Lam Nguyen  <https://orcid.org/0000-0002-7794-9439>

REFERENCES

- Atkinson R, Baulch DL, Cox RA, et al. Evaluated kinetic and photochemical data for atmospheric chemistry: volume I—gas phase reactions of O_x, HO_x, NO_x and SO_x species. *Atmos Chem Phys*. 2004;4:1461-1738.
- Baulch DL, Bowman CT, Cobos CJ, et al. Evaluated kinetic data for combustion modeling: supplement II. *J Phys Chem Ref Data*. 2005;34(3):757-1397.
- Burkholder JB, Sander SP, Abbatt J, Barker JR, Huie RE, Kolb CE, Kurylo MJ, Orkin VL, Wilmouth DM, Wine PH. Chemical kinetics and photochemical data for use in atmospheric studies, Evaluation No. 18, JPL Publication 15-10, Jet Propulsion Laboratory, Pasadena, 2015. <http://jpldataeval.jpl.nasa.gov>.
- Atkinson R, Baulch DL, Cox RA, et al. Task Group on Atmospheric Chemical Kinetic Data Evaluation. 2019. International Union of Pure and Applied Chemistry. <http://iupac.pole-ether.fr>.
- Li Y, Francisco JS. High level ab initio studies on the excited states of HOCO radical. *J Chem Phys*. 2000;113:7963-7970.
- Yu H-G, Muckerman JT, Sears TJ. A theoretical study of the potential energy surface for the reaction OH+CO → H+CO₂. *Chem Phys Lett*. 2001;349(5-6):547-554.
- Francisco JS, Muckerman JT, Yu H-G. HOCO radical chemistry. *Acc Chem Res*. 2010;43:1519-1526.
- Conte R, Houston PL, Bowman JM. Communication: a benchmark-quality, full-dimensional ab initio potential energy surface for Ar-HOCO. *J Chem Phys*. 2014;140:151101.
- Kudla K, Schatz GC, Wagner AF. A quasi-classical trajectory study of the OH+CO reaction. *J Chem Phys*. 1991;95(3):1635-1647.
- Bradley KS, Schatz GC. A quasiclassical trajectory study of H+CO₂: angular and translational distributions; and OH angular momentum alignment. *J Chem Phys*. 1997;106(20):8464-8472.
- Corchado JC, Espinosa-Garcia J, Li J, Guo H. CO₂ vibrational state distributions from quasi-classical trajectory studies of the HO + CO → H + CO₂ reaction and H + CO₂ inelastic collision. *J Phys Chem A*. 2013;117:11648-11654.
- Hernandez MI, Clary DC. A study of HOCO resonances in the OH+CO⁻]CO₂+H reaction. *J Chem Phys*. 1994;101(4):2779-2784.
- McCormack DA, Kroes GJ. Converged five-dimensional quantum calculations for OH plus CO → H+CO₂. *J Chem Phys*. 2002;116(10):4184-4191.
- Wang J, Li J, Ma i, Guo H. Full-dimensional characterization of photoelectron spectra of HOCO⁻ and DOCO⁻ and tunneling facilitated decay of HOCO prepared by anion photodetachment. *J Chem Phys*. 2014;140:184314.
- Fu B, Zhang DH. Ab initio potential energy surfaces and quantum dynamics for polyatomic bimolecular reactions. *J Chem Theory Comput*. 2018;14:2289-2303.
- Zhu RS, Diau EGW, Lin MC, Mebel AM. A computational study of the OH(OD) plus CO reactions: effects of pressure; temperature; and quantum-mechanical tunneling on product formation. *J Phys Chem A*. 2001;105(50):11249-11259.
- Wagner AF, Dawes R, Continetti RE, Guo H. Theoretical/experimental comparison of deep tunneling decay of quasi-bound H(D)OCO to H(D) + CO₂. *J Chem Phys*. 2014;141:054304.
- Weston RE, Jr, Nguyen TL, Stanton JF, Barker JR. HO + CO reaction rates and H/D kinetic isotope effects: master equation models with ab Initio SCTST rate constants. *J Phys Chem A*. 2013;117:821-835.
- Nguyen TL, Xue B, Weston RE, Jr, Barker JR, Stanton JF. Reaction of HO with CO: tunneling is indeed important. *J Phys Chem Lett*. 2012;3:1549-1553.
- Meng Q, Chen J. Ring-polymer molecular dynamics study on rate coefficient of the barrierless OH + CO system at low temperature. *J Chem Phys*. 2019;150: 044307.
- Miller WH. Semi-classical theory for non-separable systems: construction of “good” action-angle variables for reaction rate constants. *Faraday Discuss Chem Soc*. 1977;62:40-46.
- Hernandez R, Miller WH. Semiclassical transition state theory. *Chem Phys Lett*. 1993;214(2):129-136.
- Nguyen TL, Stanton JF, Barker JR. A practical implementation of semi-classical transition state theory for polyatomics. *Chem Phys Lett*. 2010;499:9-15.
- Nguyen TL, Stanton JF, Barker JR. Ab initio reaction rate constants computed using semiclassical transition-state theory: HO + H₂ → H₂O + H and isotopologues. *J Phys Chem A*. 2011;115:5118-5126.
- Nguyen TL, Barker JR, Stanton JF. Atmospheric reaction rate constants and kinetic isotope effects computed using the HEAT Protocol and semi-classical transition state theory. In: Barker JR, Steiner AL, Wallington TJ, eds., *Advances in Atmospheric Chemistry*. Singapore: World Scientific; 2017:403-492.
- Tajti A, Szalay PG, Csaszar AG, et al. HEAT: high accuracy extrapolated ab initio thermochemistry. *J Chem Phys*. 2004;121(23):11599-11613.
- Bomble YJ, Vazquez J, Kallay M, et al. High-accuracy extrapolated ab initio thermochemistry. II. Minor improvements to the protocol and a vital simplification. *J Chem Phys*. 2006;125:064108.

28. Harding ME, Vazquez J, Ruscic B, Wilson AK, Gauss J, Stanton JF. High-accuracy extrapolated ab initio thermochemistry. III. Additional improvements and overview. *J Chem Phys*. 2008;128:114111.
29. Stanton JF, Gauss J, Harding ME, et al. CFOUR, a quantum chemical program package. 2016. <http://www.cfour.de/>
30. Bui TQ, Bjork BJ, Changala PB, et al. Direct measurements of DOCO isomers in the kinetics of OD + CO. *Sci Adv*. 2018;4.
31. McCarthy MC, Martinez O, Jr, McGuire BA, Crabtree KN, Martin-Drumel M-A, Stanton JF. Isotopic studies of trans and cis-HOCO using rotational spectroscopy: formation, chemical bonding, and molecular structures. *J Chem Phys*. 2016;144:124304.
32. Johnson CJ, Harding ME, Poad BLJ, Stanton JF, Continetti RE. Communication: the electron affinities, well depths and vibrational spectroscopy of cis- and trans-HOCO. *J Am Chem Soc*. 2011;133:19606-19609.
33. Caravan RL, Shannon RJ, Lewis T, Blitz MA, Heard DE. Measurements of rate coefficients for reactions of OH with ethanol and propan-2-ol at very low temperatures. *J Phys Chem A*. 2015;119:7130-7137.
34. Acharyya K, Herbst E, Caravan RL, Shannon RJ, Blitz MA, Heard DE. The importance of OH radical-neutral low temperature tunnelling reactions in interstellar clouds using a new model. *Mol Phys*. 2015;113:2243-2254.
35. Nguyen TL, Ruscic B, Stanton JF. A master equation simulation for the $\dot{\text{O}}\text{H} + \text{CH}_3\text{OH}$ reaction. *J Chem Phys*. 2019;150:084105.
36. Bjork BJ, Bui TQ, Heckl OH, et al. Direct frequency comb measurement of OD + CO \rightarrow DOCO kinetics. *Science*. 2016;354:444-448.
37. Bui TQ, Bjork BJ, Changala PB, Heckl OH, Spaun JYB. OD + CO \rightarrow D + CO₂ branching kinetics probed with time-resolved frequency comb spectroscopy. *Chem Phys Lett*. 2017;683:91-95.
38. Thorpe JH, Lopez CA, Nguyen TL, et al. High-accuracy extrapolated ab initio thermochemistry. IV. A modified recipe for computational efficiency. *J Chem Phys*. 2019;150:224102.
39. Jeffrey SJ, Gates KE, Smith SC. Full iterative solution of the two-dimensional master equation for thermal unimolecular reactions. *J Phys Chem A*. 1996;100:7090-7096.
40. Robertson SH, Pilling MJ, Gates KE, Smith SC. Application of inverse iteration to 2-dimensional master equations. *J Comput Chem*. 1997;18:1004-1010.
41. Venkatesh PK, Dean AM, Cohen MH, Carr RW. Master equation analysis of intermolecular energy transfer in multiple-well, multiple-channel unimolecular reactions. I Basic theory. *J Chem Phys*. 1997;107(21):8904-8916.
42. Venkatesh PK, Dean AM, Cohen MH, Carr RW. Master equation analysis of intermolecular energy transfer in multiple-well, multiple-channel unimolecular reactions. II. Numerical methods and application to the mechanism of the C₂H₅+O₂ reaction. *J Chem Phys*. 1999;111(18):8313-8329.
43. Frankcombe TJ, Smith SC. Numerical solution methods for large, difficult kinetic master equations. *Theor Chem Acc*. 2009;124:303-317.
44. Jasper AW, Pelzer KM, Miller JA, Kamarchik E, Harding LB, Klippenstein SJ. Predictive a priori pressure-dependent kinetics. *Science*. 2014;346:1212-1215.
45. Robertson SH. In: Robertson SH, ed. Foundations of the master equation. In *Unimolecular Kinetics: Parts 2 and 3: Collisional Energy Transfer and the Master Equation*. Amsterdam, the Netherlands: Elsevier; 2019:299-361. <https://doi.org/10.1016/B978-0-444-64207-3.00005-6>. Editor.
46. Nguyen TL, Stanton JF. Pragmatic solution for a fully E,J-resolved master equation. *J Phys Chem A*. 2020;124:2907-2918.
47. Jasper AW. Microcanonical rate constants for unimolecular reactions in the low-pressure limit. *J Phys Chem A*. 2020;124:1205-1226.
48. Smith SC, Gilbert RG. Angular momentum conservation in unimolecular and recombination reactions. *Int J Chem Kinet*. 1988;20:307-329.
49. Gilbert RG, Smith SC. *Theory of Unimolecular and Recombination Reactions*. Oxford, UK: Blackwell Scientific; 1990.
50. Smith IWM. Mechanism of OH + CO reaction and stability of HOCO radical. *Chem Phys Lett*. 1977;49(1):112-115.
51. Atkinson R, Baulch DL, Cox RA, et al. Evaluated kinetic and photochemical data for atmospheric chemistry: volume II – gas phase reactions of organic species. *Atmos Chem Phys*. 2006;6:3625-4055.
52. Atkinson R, Baulch DL, Cox RA, et al. Evaluated kinetic and photochemical data for atmospheric chemistry: volume III – gas phase reactions of inorganic halogens. *Atmos Chem Phys*. 2007;7:981-1191.
53. Forster R, Frost M, Fulle D, et al. High-pressure range of the addition of HO to HO; NO; NO₂; and CO .1. Saturated laser-induced fluorescence measurements at 298 K. *J Chem Phys*. 1995;103(8):2949-2958.
54. Fulle D, Hamann HF, Hippler H, Troe J. High pressure range of addition reactions of HO. 2. Temperature and pressure dependence of the reaction HO + CO \rightleftharpoons HOCO \rightarrow H + CO₂. *J Chem Phys*. 1996;105(3):983-1000.
55. Smith IWM. Relaxation in collisions of vibrationally excited molecules with potentially reactive atoms. *Acc Chem Res*. 1976;9:161-168.
56. Fernando RP, Smith IWM. Vibrational-relaxation of NO by atomic oxygen. *Chem Phys Lett*. 1979;66(2):218-222.
57. Fernando RP, Smith IWM. Relaxation of NO($v = 1$) by radical species. *J Chem Soc, Faraday Trans 2*. 1981;77:459-468.
58. Smith IWM, Williams MD. Vibrational-relaxation of OH($v = 1$) and OD($v = 1$) by HNO₃, DNO₃, H₂O, NO, and NO₂. *J Chem Soc, Faraday Trans 2*. 1985;81:1849.
59. Blitz MA, Salter RJ, Heard DE, Seakins PW. An experimental study of the kinetics of OH/OD($v = 1,2,3$) + SO₂: the limiting high-pressure rate coefficients as a function of temperature. *J Phys Chem A*. 2017;121:3175-3183.
60. Liu Y, Sander SP. Rate constant for the OH + CO reaction at low temperatures. *J Phys Chem A*. 2015;119:10060-10066.
61. Golden DM, Smith GP, McEwen AB, et al. OH(OD)+CO: measurements and an optimized RRKM fit. *J Phys Chem A*. 1998;102(44):8598-8606.
62. McCabe DC, Gierczak T, Talukdar RK, Ravishankara AR. Kinetics of the reaction OH plus CO under atmospheric conditions. *GeoRL*. 2001;28(16):3135-3138.
63. Greenslade ME, Tsiouris M, Bonn RT, Lester MI. Electronic spectroscopy of the OH-CO reactant complex. *Chem Phys Lett*. 2002;354(3-4):203-209.
64. Brunning J, Derbyshire DW, Smith IWM, Williams MD. Kinetics of OH($v = 0; 1$) and OD($v = 0; 1$) with CO and the mechanism of the OH + CO reaction. *J Chem Soc, Faraday Trans 2*. 1988;84:105-119.

65. Hill E, Van Vleck JH. On the quantum mechanics of the rotational distortion of multiplets in molecular spectra. *Phys Rev.* 1929;32:250-272.
66. Masoumpour MS, Daryanavard M. The kinetics and dynamics of the multichannel multiwell reaction of CO(Σ^+) with OH(Σ^+): theoretical investigation. *SN Appl Sci.* 2020;2:481.
67. Barker JR. Multiple-well, multiple-path unimolecular reaction systems. I. MultiWell computer program suite. *Int J Chem Kinet.* 2001;33(4):232-245.
68. Barker JR, Nguyen TL, Stanton JF, et al. *MultiWell-2019 Software Suite*. Ann Arbor, MI: University of Michigan; 2019. <https://clasp-research.engin.umich.edu/multiwell/>
69. Miller WH. Unified statistical model for "complex" and "direct" reaction mechanisms. *J Chem Phys.* 1976;65:2216-2223.
70. Barker JR. Monte-Carlo calculations on unimolecular reactions, energy-transfer, and IR-multiphoton decomposition. *Chem Phys.* 1983;77(2):301-318.
71. Barker JR. Monte Carlo stochastic simulation of the master equation for unimolecular reaction systems. In: Robertson SH, ed. *Unimolecular Kinetics. Parts 2 and 3: Collisional Energy Transfer and The Master Equation*. Amsterdam, the Netherlands: Elsevier; 2019:409-463. <https://doi.org/10.1016/B978-0-444-64207-3.00007-X>.
72. Brooke JSA, Bernath PF, Western CM, et al. Line strengths of rovibrational and rotational transitions in the X $^2\Pi$ ground state of OH. *J Quant Spectrosc Radiat Transf.* 2016;168:142-157.
73. Liu J, Shen Y, Asthana A, Cheng L. Two-component relativistic coupled-cluster methods using mean-field spin-orbit integrals. *J Chem Phys.* 2018;148.
74. Pond BV, Lester MI. Decay dynamics of the vibrationally activated OH-CO reactant complex. *J Chem Phys.* 2003;118:2223-2234.
75. Marshall MD, Pond BV, Lester MI. Intermolecular vibrations of the hydrogen bonded OH-CO reactant complex. *J Chem Phys.* 2003;118:1196-1205.
76. Miller JA, Klippenstein SJ, Raffy C. Solution of some one- and two-dimensional master equation models for thermal dissociation: the dissociation of methane in the low pressure limit. *J Phys Chem A.* 2002;106(19):4904-4913.
77. King KD, Barker JR. Experiments on collisional energy transfer. In: Robertson SH, ed. *Unimolecular Kinetics. Parts 2 and 3: Collisional Energy Transfer and The Master Equation*. Amsterdam, the Netherlands: Elsevier; 2019:3-62. <https://doi.org/10.1016/B978-0-444-64207-3.00001-9>.
78. Lendvay G. Classical trajectory studies of collisional energy transfer. In: Robertson SH, ed. *Unimolecular Kinetics: Parts 2 and 3: Collisional Energy Transfer and the Master Equation*. Amsterdam, the Netherlands: Elsevier; 2019:110-272. <https://doi.org/10.1016/B978-0-444-64207-3.00003-2>.
79. Robertson SH. Parametric models. In: Robertson SH, ed. *Unimolecular Kinetics: Parts 2 and 3: Collisional Energy Transfer and the Master Equation*. Amsterdam, the Netherlands: Elsevier; 2019:273-295. <https://doi.org/10.1016/B978-0-444-64207-3.00004-4>.
80. Marcus RA. Unimolecular dissociations and free radical recombination reactions. *J Chem Phys.* 1952;20(3):359-364.
81. Waage EV, Rabinovitch BS. Centrifugal effects in reaction rate theory. *Chem Rev.* 1970;70:377-387.
82. Holbrook KA, Pilling MJ, Robertson SH. *Unimolecular Reactions*. 2 ed. Chichester, UK: Wiley; 1996.
83. Forst W. *Unimolecular Reactions. A Concise Introduction*. Cambridge, UK: Cambridge University Press; 2003.
84. Baer T, Hase WL. *Unimolecular Reaction Dynamics. Theory and Experiments*. New York: Oxford University Press; 1996.
85. Zhu L, Hase WL. Comparison of models for calculating the RRKM unimolecular rate constant $k(E,J)$. *Chem Phys Lett.* 1990;175(1,2):117-124.
86. Aubanel EE, Wardlaw DM, Zhu L, Hase WL. Role of angular momentum in statistical unimolecular rate theory. *Int Rev Phys Chem.* 1991;10(3):249-286.
87. Zhu L, Chen W, Hase WL, Kaiser EW. Comparison of models for treating angular momentum in RRKM calculations with vibrator transition states. Pressure and temperature dependence of the Cl + C $_2$ H $_2$ association. *J Phys Chem.* 1993;97:311-322.
88. Song K, Hase WL. Role of state specificity in the temperature- and pressure-dependent unimolecular rate constants for HO $_2$ \rightarrow H + O $_2$ dissociation. *J Phys Chem A.* 1998;102:1292-1296.
89. Hase WL. Some recent advances and remaining questions regarding unimolecular rate theory. *Acc Chem Res.* 1998;31:659-665.
90. Song K, Sun LP, Hase WL, Grebenshchikov SY, Schinke R. Relationship between mode specific and thermal unimolecular rate constants for HOCl \rightarrow OH + Cl Dissociation. *J Phys Chem A.* 2002;106:8339-8344.
91. McGivern WS, North SW. Treatment of the K-quantum number in unimolecular reaction theory: insights from product correlations. *J Am Chem Soc.* 2002;124:4472-14477.
92. Nguyen TL, Stanton JF. Three-dimensional master equation (3DME) approach. *J Phys Chem A.* 2018;122:7757-7767.
93. Penner AP, Forst W. Transfer of vibrational-rotational energy in thermal reactions: approximations, application to diatomics. *Chem Phys.* 1975;11:243-251.
94. Penner AP, Forst W. Transfer of vibrational-rotational energy in thermal reactions: application to polyatomics. *Chem Phys.* 1976;13:51-64.
95. Nguyen TL, Stanton JF. A steady-state approximation to the two-dimensional master equation for chemical kinetics calculations. *J Phys Chem A.* 2015;119(28):7627-7636.
96. Miller JA, Klippenstein SJ. Master equation methods in gas phase chemical kinetics. *J Phys Chem A.* 2006;110:10528-10544.
97. Marcus RA. Dissociation and isomerization of vibrationally excited species.III. *J Chem Phys.* 1965;43(8):2658-2661.
98. Barker JR. Collisional energy transfer probability densities $P(E,J;E',J')$ for monatomics colliding with large molecules. *J Phys Chem A.* 2010;114:10619-10633.
99. Smith IWM, Ravishankara AR. Role of hydrogen-bonded intermediates in the bimolecular reactions of the hydroxyl radical. *J Phys Chem A.* 2002;106(19):4798-4807.
100. Nguyen TL, Stanton JF. Ab initio thermal rate calculations of HO + HO = O(3P) + H $_2$ O reaction and isotopologues. *J Phys Chem A.* 2013;117:2678-2686.
101. Perry DS. Time scales and mechanisms of intramolecular energy redistribution. In: Mullin A, Schatz GC, eds. *Highly Excited States: Relaxation, Reaction, and Structure*. Washington, DC: American Chemical Society; 1997:70-80.

102. Leitner DM. Quantum ergodicity and energy flow in molecules. *AdPhy*. 2015;64(4):445-517.
103. Mullin AS, Schatz GC. Dynamics of highly excited states in chemistry: An overview. In: Mullin A, Schatz GC, eds. *Highly Excited Molecules: Relaxation, Reaction, and Structure*. Washington, DC: American Chemical Society; 1997:2-25.
104. McDonald JD. Creation and disposal of vibrational energy in polyatomic molecules. *Ann Rev Phys Chem*. 1979;30:29-50.
105. Nesbitt DJ, Leone SR. Infrared fluorescence studies of intramolecular vibrational relaxation in C₁-C₄ hydrocarbons following pulsed laser excitation of the first CH stretch overtone. *Chem Phys Lett*. 1982;87:123-127.
106. Stewart GM, McDonald JD. Intramolecular vibrational relaxation from C-H stretch fundamentals. *J Chem Phys*. 1983;78:3907-3915.
107. Kulp T, Ruoff RS, McDonald JD. Limits on the lifetimes of intramolecular rovibrational relaxation. *J Chem Phys*. 1985;2175-2179.
108. Brumbaugh DV, Kenny JE, Levy DH. Vibrational predissociation and intramolecular vibrational relaxation in electronically excited s-tetrazine-argon van der Waals complex. *J Chem Phys*. 1983;78(6):3415.
109. Ravishankara AR, Thompson RL. Kinetic-study of the reaction of OH with CO from 250 K to 1040 K. *Chem Phys Lett*. 1983;99(5-6):377-381.
110. Frost MJ, Salh JS, Smith IWM. Vibrational-state distribution of CO₂ produced in the reaction between OH radicals and CO. *J Chem Soc, Faraday Trans*. 1991;87(7):1037-1038.
111. Frost MJ, Sharkey P, Smith IWM. Reaction between OH (OD) radicals and CO at temperatures down to 80 K: experiment and theory. *J Phys Chem*. 1993;97(47):12254-12259.
112. Scott AP, Radom L. Harmonic vibrational frequencies: an evaluation of Hartree-Fock, Møller-Plesset, quadratic configuration interaction, density functional theory, and semiempirical scale factors. *J Phys Chem*. 1966;100:16502-16513.
113. Pople JA, Scott AP, Wong MW, Radom L. Scaling factors for obtaining fundamental vibrational frequencies and zero-point energies from HF/6-31G* and MP2/6-31G* harmonic frequencies. *Isr J Chem*. 1993;33:345-350.
114. Alecu IM, Zheng J, Zhao Y, Truhlar DG. Computational thermochemistry: scale factor databases and scale factors for vibrational frequencies obtained from electronic model chemistries. *J Chem Theor Comp*. 2010;6:2872-2887.
115. McCaslin L, Stanton J. Calculation of fundamental frequencies for small polyatomic molecules: a comparison between correlation consistent and atomic natural orbital basis sets. *Mol Phys*. 2013;111:1492-1496.
116. Hippler H, Rahn R, Troe J. Temperature and pressure dependence of ozone formation rates in the range 1-1000 bar and 90-370 K. *J Chem Phys*. 1990;93:6560-6569.
117. Luther K, Oum K, Troe J. Study of the recombination reaction CCl₃+O₂ (+M) →. *J Phys Chem A*. 2001;105(23):5535-5541.
118. Troe J. Toward a quantitative analysis of association reactions in the atmosphere. *Chem Rev*. 2003;103:4565-4576.
119. Liu JY, Barker JR. On the chaperon mechanism: application to ClO+ClO(+N₂) → ClOCl(+N₂). *J Phys Chem A*. 2007;111(35):8689-8698.

SUPPORTING INFORMATION

Additional supporting information may be found online in the Supporting Information section at the end of the article.

How to cite this article: Barker JR, Stanton JF, Nguyen TL. Semiclassical transition state theory / master equation kinetics of HO + CO: performance evaluation. *Int J Chem Kinet*. 2020;52:1022-1045. <https://doi.org/10.1002/kin.21420>